Soil Erosion Risk Assessment in Italy

J.M. van der Knijff, R.J.A. Jones,
L. Montanarella

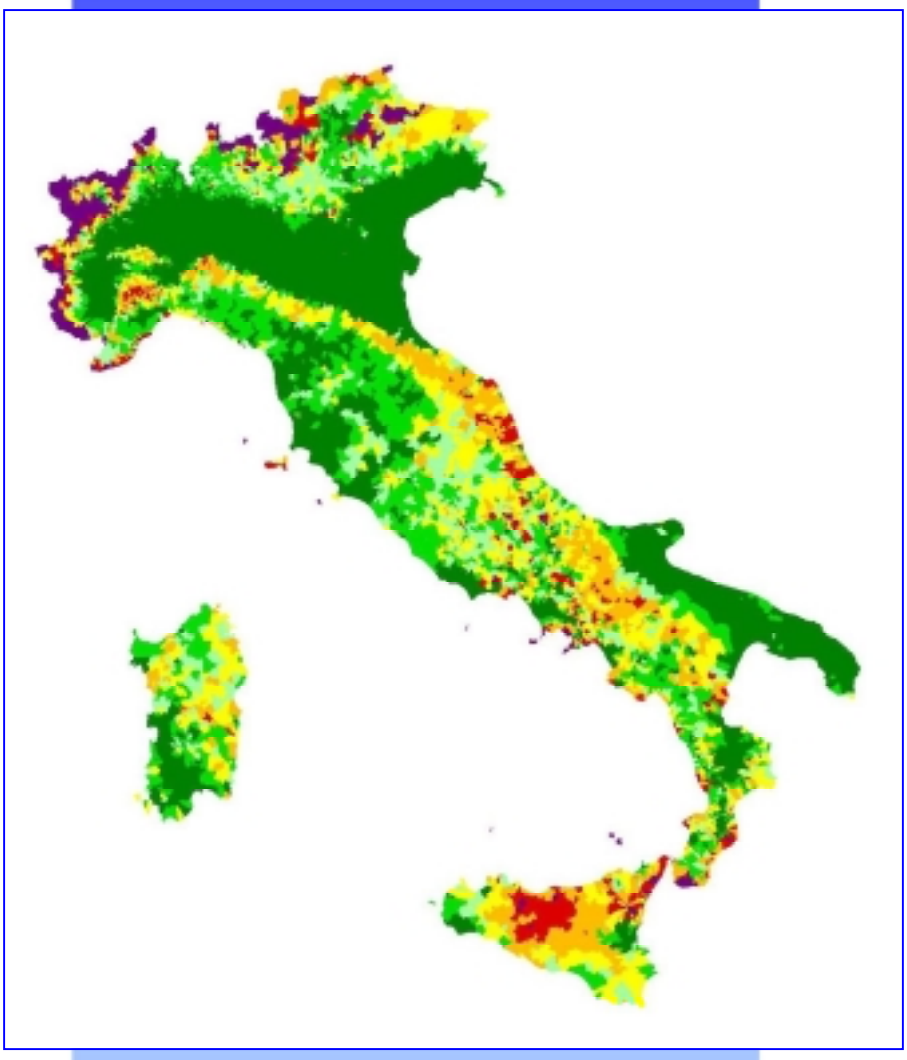

EUROPEAN SOIL BUREAU
EUROPEAN COMMISSION

JOINT RESEARCH CENTRE
EUROPEAN COMMISSION

Space Applications Institute

1999

EUR 19022EN

Contents

1. Introduction

Soil erosion by water is a widespread problem throughout Europe. A report for the Council of Europe, using revised GLASOD data (Oldeman *et al.*, 1991; Van Lynden, 1995), provides an overview of the extent of soil degradation in Europe. Some of the findings are shown in the Table 1.1, but these figures shown are only a rough approximation of the area affected by soil degradation.

Table 1.1. Human-induced Soil Degradation in Europe[1] (M ha)

WATER EROSION	**Light**	**Moderate**	**Strong**	**Extreme**	**Total**
Loss of Topsoil	18.9	64.7	9.2	-	92.8
Terrain Deformation	2.5	16.3	0.6	2.4	21.8
Total:	21.4	81.0	9.8	2.4	114.5 (52.3%)

[1] Includes the European part of the former Soviet Union.

However, Table 1.1 indicates the importance of water erosion in Europe in terms of area affected. The most dominant effect is the loss of topsoil, which is often not conspicuous but nevertheless potentially very damaging. Physical factors like climate, topography and soil characteristics are important in the process of soil erosion. In part, this explains the difference between the severe water erosion problem in Iceland but the much less severe erosion in Scandinavia where the climate is less harsh and the soils are less erodible (Fournier, 1972).

The Mediterranean region is particularly prone to erosion. This is because it is subject to long dry periods followed by heavy bursts of erosive rainfall, falling on steep slopes with fragile soils, resulting in considerable amounts of erosion. This contrasts with NW Europe where soil erosion is slight because rain falling on mainly gentle slopes is evenly distributed throughout the year. Consequently, the area affected by erosion in northern Europe is much more restricted in its extent than in southern Europe.

In parts of the Mediterranean region, erosion has reached a stage of irreversibility and in some places erosion has practically ceased because there is no more soil left. With a very slow rate of soil formation, any soil loss of more than 1 t/ha/yr can be considered as irreversible within a time span of 50-100 years. Losses of 20 to 40 t/ha in individual storms, that may happen once every two or three years, are measured regularly in Europe with losses of more than 100 t/ha in extreme events (Morgan, 1992). It may take some time before the effects of such erosion become noticeable, especially in areas with the deepest and most fertile soils or on heavily fertilised land. However, this is all the more dangerous because, once the effects have become obvious, it is usually be too late to do anything about it.

The main causes of soil erosion are still inappropriate agricultural practices, deforestation, overgrazing and construction activities (Yassoglou *et al.*, 1998). Increasing the awareness amongst scientists and policy makers about the soil degradation problem in Europe is now an urgent requirement. The identification of

areas that are vulnerable to soil erosion can be helpful for improving our knowledge about the extent of the areas affected and, ultimately, for developing measures to keep the problem under control whenever possible.

1.1 Italy Project

In an attempt to quantify erosion in the Mediterranean using modern digital techniques, a project was initiated in Italy that aims to assess erosion risk at national level. The end product is a set of maps that can be used as an aid to identifying regions that are prone to erosion

The project forms part of the Soil Map of Italy Project, a major initiative by the Italian Ministry of Agriculture aimed at compiling a 1:250,000 scale soil map and associated database for Italy. This is urgently needed for environmental protection and planning the sustainable use of land resources in the country. Recent disasters – land slipping and flooding – have highlighted the importance of having good detailed soil information in a modern industrial state such as Italy for combating such events. This study addresses rill- and inter-rill erosion only. Other forms of erosion are also important in Italy, for example gully erosion, landslides and, to a lesser extent, wind erosion. However, these types of erosion are not addressed in this study, but they should be addressed some time in the future.

This report gives a detailed technical description of the erosion part of the Italy project. An overview of the various methods that can be used to assess soil erosion risk at the regional scale and larger is given in Chapter 2. Chapter 3 gives a general description of the methods used in this study. A more detailed description can be found in Chapters 4-7, along with an explanation of the data sources and processing. A discussion of the results can be found in Chapter 8.

2. Assessing soil erosion risk

For assessing soil erosion risk, various approaches can be adopted. A distinction can be made here between *expert*-based and *model*-based approaches.

2.1 Expert based methods

An example of an expert-based approach is the soil erosion risk map of Western Europe by De Ploey (1989). The map was produced by various experts who delineated areas where, according to their judgement, erosion processes are important. A limitation of this approach is that the author does not give a clear-cut definition of the criteria according to which areas were delineated (Yassoglou *et al.*, 1998).

Factorial scoring is another approach that can be used to assess erosion risk (Morgan, 1995). An example is the CORINE soil erosion risk assessment of the Mediterranean region (CORINE, 1992). The analysis is based on factorial scores for soil erodibility (4 classes), erosivity (3 classes) and slope angle (4 classes). The scores are multiplied, giving a combined score that represents potential erosion risk. To assess actual soil erosion risk, the potential erosion risk map is combined with a land cover factor (2 classes).

Montier *et al.* (1998) developed an expert-based method for the whole of France. As with CORINE, the method is based on scores that are assigned to factors related to land cover (9 classes), the soil's susceptibility to surface crusting (4 classes), slope angle (8 classes) and erodibility (3 classes). An interesting feature of their method is that it takes into account the different types of erosion that occur on cultivated areas, vineyards, mountainous areas and the Mediterranean. This way, the interaction between soil, vegetation, slope and climate is accounted for to some extent.

A problem with most methods based on scoring is that the results are affected by the way the scores are defined. In addition to this, classifying the source data in e.g. slope classes results in information loss, and the results of the analyses may depend strongly on the class limits and the number of classes used. Moreover, unless some kind of weighting is used each factor is given equal weight, which is not realistic. If one decides to use some weighting, choosing realistic values for the weights may be difficult. The way in which the various factors are combined into classes that are functional with respect to erosion risk (addition, multiplication) may pose problems also (Morgan, 1995). Finally, as factorial scoring produces qualitative erosion classes, the interpretation of these classes can be difficult.

2.2 Model based methods

A wide variety of models are available for assessing soil erosion risk. Erosion models can be classified in a number of ways. One may make a subdivision based on the time scale for which a model can be used: some models are designed to predict

long-term annual soil losses, while others predict single storm losses (event-based). Alternatively, a distinction can be made between lumped models that predict erosion at a single point, and spatially distributed models. Another useful division is the one between empirical and physically-based models. The choice for a particular model largely depends on the purpose for which it is intended and the available data, time and money.

Jäger (1994) used the empirical Universal Soil Loss Equation (USLE) to assess soil erosion risk in Baden-Württemberg (Germany). De Jong (1994) used the Morgan, Morgan and Finney model (Morgan *et al.*, 1984) as a basis for his SEMMED model. Input variables are derived from standard meteorological data, soil maps, multi-temporal satellite imagery, digital elevation models and a limited amount of field data. This way, erosion risk can be assessed over large, spatially diverse areas without the need for extensive field surveys. So far the SEMMED model has been used to produce regional erosion risk maps of parts of the Ardêche region and the Peyne catchment in Southern France (De Jong, 1994, De Jong *et al.*, 1998).

Kirkby and King (1998) assessed soil erosion risk for the whole of France using a model-based approach. Their model provides a simplified representation of erosion in an individual storm. The model contains terms for soil erodibility, topography and climate. All storm rainfall above a critical threshold (whose value depends on soil properties and land cover) is assumed to contribute to runoff, and erosion is assumed to be proportional to runoff. Monthly and annual erosion estimates are obtained by integrating over the frequency distribution of rainstorms.

Several problems arise when applying quantitative models at regional or larger scale. First, most erosion models were developed on a plot or field scale, which means that they are designed to provide point estimates of soil loss. When these models are applied over large areas the model output has to be interpreted carefully. One cannot expect that a model that was designed to predict soil loss on a single agricultural field produces accurate erosion estimates when applied to the regional scale on a grid of say 50 meter pixels or coarser. One should also be aware of which processes are actually being modeled. For example, the well-known Universal Soil Loss Equation was developed to predict rill- and inter-rill erosion only. Therefore, one cannot expect this model to perform well in areas where gully erosion is the dominant erosion type, let alone mass-movements like landslides and rockfalls.

Also, at the regional scale it is usually impossible to determine the model's input data (like soil and vegetation parameters) directly in the field. Usually, the model parameters are approximated by assigning values to mapping units on a soil or vegetation map, or through regression equations between e.g. vegetation cover and some satellite-derived spectral index. In general however, this will yield parameter values that are far less accurate than the results of a field survey. Because of all this, the relative soil loss values produced by models at this scale are generally more reliable than the absolute values. This is not necessarily a problem, as long as one is aware that the model results give a broad overview of the general pattern of the relative differences, rather than providing accurate absolute erosion rates. Because of this, the availability of input data is probably the most important consideration when selecting an erosion model at the regional/national scale. It would not make sense to use a sophisticated model if sufficient input data are not available. In the

latter case, the only way to run the model would be to assume certain variables and model parameters to be constant. However, the results would probably be less reliable than the results that would have been obtained with a simpler model that requires less input data (De Roo, 1993). Also, uncertainties in the model's input propagate throughout the model, so one should be careful not to use an 'over-parameterised' model when the quality of the input data is poor.

Perhaps the biggest problem with erosion modelling is the difficulty of validating the estimates produced. At the regional and larger scale, virtually no reliable data exist for comparing estimates with actual soil losses. King *et al.* (1999) attempted to validate an erosion risk assessment for France by correlating soil loss with the occurrence of mudflows. However, other processes are involved here and such comparisons do not substitute for 'real' measurements.

3. Universal Soil Loss Equation

3.1 Introduction

For this study a model-based approach was used to assess soil erosion risk. As explained in Chapter 2, the availability of input data is a critical selection criterion when assessing soil erosion risk at the regional (or national) scale. Even though a wide variety of models are available for assessing soil erosion risk, most of them simply require so much input data that applying them at regional or national scale becomes problematic. The well-known Universal Soil Loss Equation (USLE) (Wischmeier & Smith, 1978) was used because it is one of the least data demanding erosion models that has been developed and it has been applied widely at different scales. The USLE is a simple empirical model, based on regression analyses of soil loss rates on erosion plots in the USA. The model is designed to estimate long-term annual erosion rates on agricultural fields. Although the equation has many shortcomings and limitations, it is widely used because of its relative simplicity and robustness (Desmet & Govers, 1996). It also represents a standardised approach.

Soil erosion is estimated using the following empirical equation:

$$A = R \cdot K \cdot L \cdot S \cdot C \qquad (3.1)$$

Where:

A : Mean (annual) soil loss
R : Rainfall erosivity factor
K : Soil erodibility factor
L : Slope factor
S : Slope length factor
C : Cover management factor

For this study, the model was run on a monthly time interval, thus taking into account the interaction between vegetation growth together with senescence over the year, and rainfall. The data sources that were used to estimate the various USLE factors are summarised in Figure 3.1. The procedures used to estimate the factors are explained in detail in the following chapters. The next paragraphs give a brief overview.

3.2 Rainfall erosivity factor

The USLE rainfall erosivity factor (*R*) for any given period is obtained by summing – for each rainstorm- the product of total storm energy (E) and the maximum 30-minute intensity (I_{30}). Unfortunately, these figures are rarely available at standard meteorological stations. Moreover, the workload involved would be rather high for any national assessment. Fortunately, long-term average R-values are often correlated with more readily available rainfall figures like annual rainfall or the

modified Fournier's index (Arnoldus, 1978). A similar approach was used to estimate *R* for Italy (Chapter 4).

3.3 Soil erodibility factor

The *K* factor is defined as the rate of soil loss per unit of *R* as measured on a unit plot ('Wischmeier plot'). It accounts for the influence of soil properties on soil loss during storm events (Renard *et al.*, 1997). The estimation of this factor is discussed in Chapter 5.

3.4 Slope- and slope length factors

The slope- and slope length factors (*S* and *L*, respectively) account for the effect of topography on soil erosion. It can be estimated from a digital elevation model (DEM), which is described in Chapter 6.

3.5 Cover management factor

The C-factor is defined as the ratio of soil loss from land with a specific vegetation to the corresponding soil loss from continuous fallow (Wischmeier & Smith, 1978). Its value depends on vegetation cover and management practices. Also, the growth stage and cover at the time when most erosive rain occurs need to be considered. For this study, *C* was estimated using a combination of satellite imagery and a land cover database, which is explained in Chapter 7.

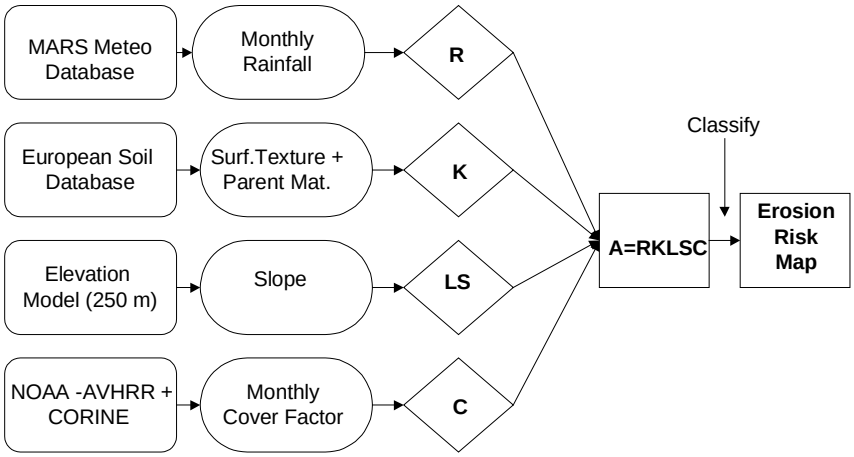

Figure 3.1 *Flowchart for creating a USLE-based erosion risk map.*

4. Rainfall Erosivity Factor

4.1 Introduction

As stated in Chapter 3, detailed information on both rainfall and rainfall intensity are needed for a direct estimation of the *R*-factor. As these data are usually unavailable for standard meteorological stations, a simplified method to estimate *R* had to be used. Zanchi (personal communication) found that for Tuscany *R* is related to annual rainfall, so that *R* can be approximated by:

$$R = a \cdot P_j \qquad (4.1)$$

Where:

P_j : Annual rainfall (mm)

When *R* is expressed in MJ.mm.ha^{-1}h^{-1}y^{-1}, *a* ranges from 1.1 to 1.5. For this study a value of 1.3 was used. The 'Tuscan equation' is based on rainfall data from 25 locations, with P_j ranging from 600 to 1200 mm. Extrapolating the formula to cover the whole of Italy is not wholly appropriate, because the characteristics of rainfall in Tuscany are not representative for other parts of the country. Nevertheless, using the 'Tuscan equation' may be justified because it is based on a wide range of annual rainfall amounts, so it may be more representative than it appears at first sight. Moreover, the erosion risk assessment presented in this study aims at giving an overview of regional patterns of erosion risk, rather than making detailed quantitative soil loss predictions. Therefore, the equation may be 'fit for purpose'.

4.2 Processing of meteorological data

Long-term monthly and annual rainfall values were computed using daily rainfall values that are stored in the MARS meteorological database (Rijks *et al.*, 1998). The locations of the meteorological stations are shown in Figure 4.1. For each station, mean annual rainfall was estimated for the period between 1-Jan 1989 and 31-Dec 1998. The annual rainfall figures were then plotted against station altitude, longitude, latitude and distance to coast. This revealed a clear relation between rainfall and latitude. Monthly regression equations predicting average monthly rainfall from latitude were established assuming a linear relationship between rainfall and latitude:

$$P_m(\varphi) = \Phi_m + \alpha_m \cdot \varphi \qquad (4.2)$$

Where:

P_m : average monthly rainfall (mm)
φ : latitude (degrees)
Φ,α : regression constants (subscripts (*m*) refer to month)

Figure 4.1 *Meteorological stations used*

In the regression analysis, only those stations at altitudes below 1000 m above sea level were used. For stations above this altitude the relationship between rainfall and latitude is less apparent because much of the winter precipitation falls as snow. The results are listed in Table 4.1. Figure 4.2 shows the variation of R^2 between rain and latitude throughout the year. The influence of latitude is negligible in early and late winter and reaches a maximum in June.

Although it is possible to use equation (4.2) directly for interpolating monthly rainfall, the variable and in some cases rather low R^2 values in Table 4.1 indicate that the results would be very poor. Another possibility would be to use a traditional interpolation technique (such as inverse-distance weighting, kriging or thin plate splines) directly on the monthly rainfall figures. However, this way the valuable extra information that is contained in the latitude data is not used. Therefore, a combination approach was adopted. Differentiation of equation (4.2) yields a local 'lapse rate' of P_m with latitude:

$$\frac{dP_m}{d\varphi} = \alpha_m \tag{4.3}$$

Integrating over $d\varphi$ gives:

$$P_m(\varphi) = C + \alpha_m \cdot \varphi \tag{4.4}$$

which is identical to (4.2), except that Φ (which is a regression constant) is replaced by the integration constant *C*. *C* is a function of monthly rainfall and latitude, and can be computed for each station simply using:

$$C = P_m(\varphi) - \alpha_m \cdot \varphi \qquad (4.5)$$

Table 4.1 Results of regression analysis

Month	R	R^2	R^2_{adj}	p	SE_{est}	Φ_m	α_m	$p(\Phi_m)$	$p(\alpha_m)$
Jan	0.64	0.41	0.395	0	18.737	267.852	-5.264	0	0
Feb	0.395	0.156	0.135	0.009	14.035	124.374	-2.033	0	0.009
Mar	0.138	0.019	-0.005	0.377	15.258	66.145	-0.717	0.055	0.377
Apr	0.665	0.443	0.429	0	23.702	-228.659	7.126	0	0
May	0.744	0.554	0.543	0	16.212	-210.302	6.087	0	0
Jun	0.892	0.795	0.79	0	17.132	-433.942	11.385	0	0
Jul	0.79	0.625	0.615	0	18.855	-311.966	8.2	0	0
Aug	0.796	0.634	0.625	0	15.262	-247.182	6.778	0	0
Sep	0.725	0.525	0.514	0	24.02	-282.743	8.519	0	0
Oct	0.377	0.142	0.121	0.013	32.163	-94.026	4.409	0.191	0.013
Nov	0.081	0.007	-0.018	0.604	28.74	52.736	0.792	0.409	0.604
Dec	0.486	0.236	0.217	0.001	25.627	271.715	-4.8	0	0.001

p = significance level; SE_{est} = standard error of regression estimate. Rows are shaded when regression equation is significant at p = 0.05. N=42 for all months.

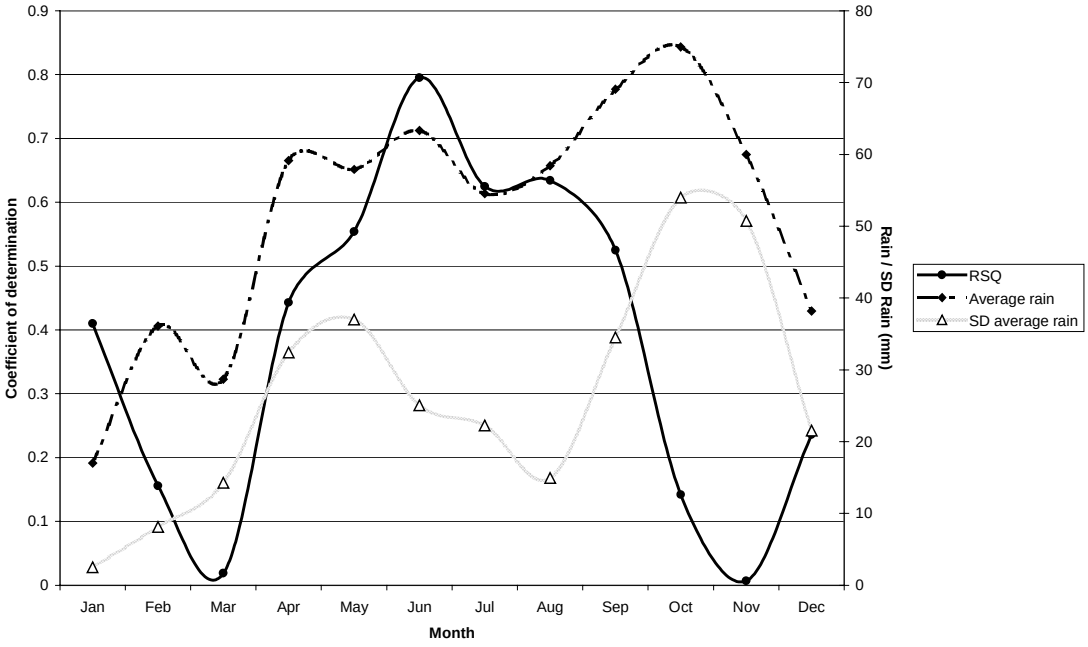

Figure 4.2 *Variation of R^2 between rainfall and latitude throughout the year*

Once *C* is computed for each station, it can be easily interpolated using any suitable interpolation technique. Subsequently, equation (4.4) can be applied to each grid cell to make a local estimate of P_m.

An example of such an interpolated rain map is shown in Figure 4.3. A thin plate spline function was used to interpolate *C*. However, Figure 4.3 clearly shows the

limitations of the method, as the locations of some of the meteorological stations can be identified easily by just looking at the pattern of the interpolated rainfall. Nevertheless, an inverse distance interpolation showed this effect even more strongly, while the density of the stations (Figure 4.1) hardly justifies the use of geostatistical techniques like kriging.

As the correlation between latitude and rainfall is negligible in early and late winter (especially November and March), the rainfall figures for these months were directly interpolated using thin plate splines without correcting for latitude at all.

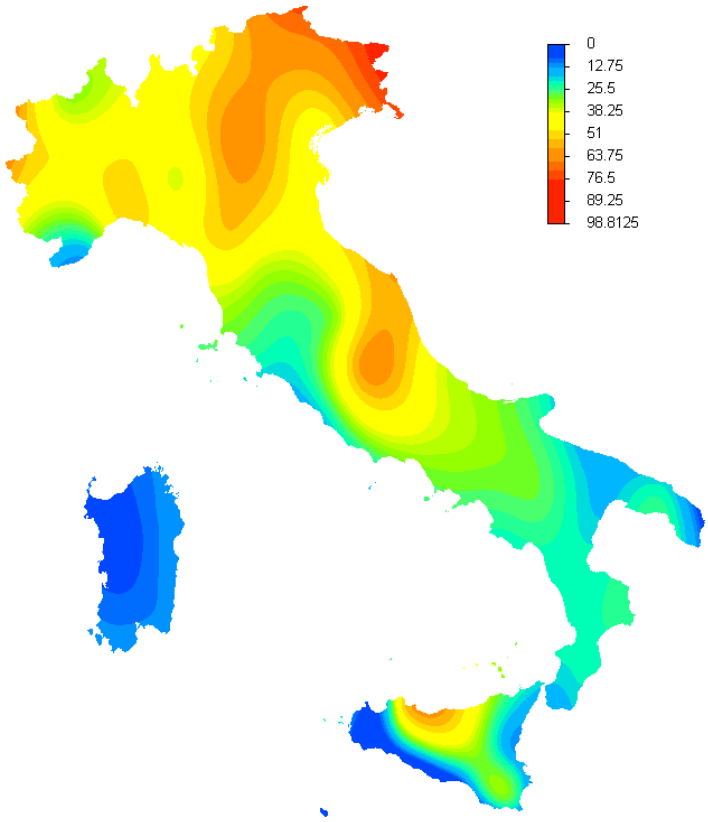

Figure 4.3 *Rainfall for August: interpolated with thin plate splines using additional information from correlation with latitude.*

4.4 Rainfall erosivity maps

Monthly erosivity maps were created by applying Equation 4.1 to each of the monthly rainfall maps. Seasonal erosivity maps are shown in figure 4.4.

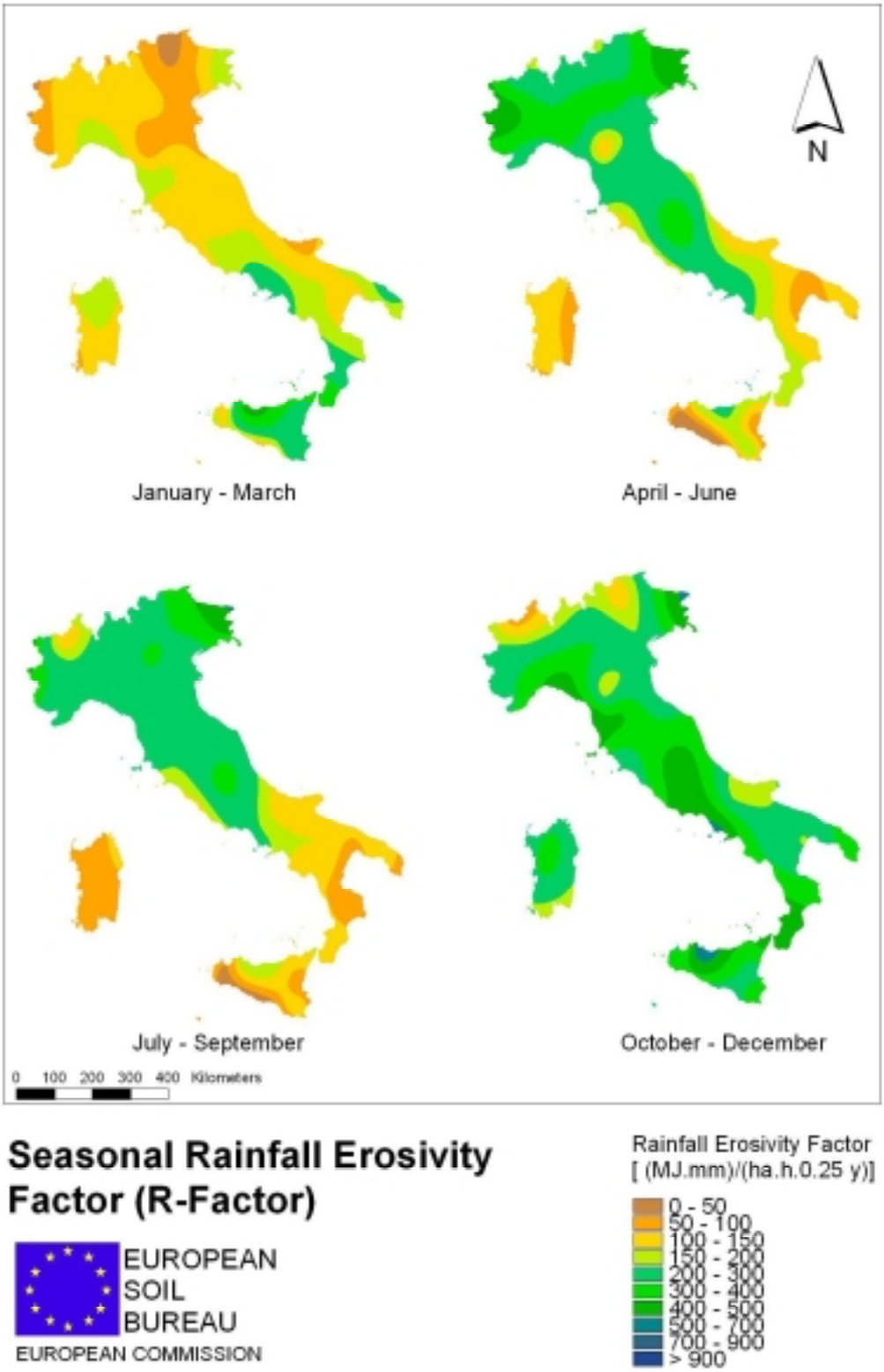

Figure 4.4 *Rainfall erosivity factor (R-factor) by season (MJ mm ha^{-1} h^{-1}0.25y^{-1}).*

5. Soil erodibility factor

5.1 Introduction

The soil erodibility factor (*K*) is usually estimated using the nomographs and formulae that are published in for example Wischmeier & Smith (1978). While these equations are suitable for large parts of the USA (for which the USLE was originally developed), they produce unreliable results when applied to soils with textural extremes as well as well-aggregated soils (Römkens et. al., 1986). Therefore, they are not ideally suited for use under European conditions.

Römkens et. al. (1986) performed a regression analysis on a world-wide dataset of all measured *K*-values, which yielded the following equation (revised in Renard *et al.*, 1997):

$$K = 0.0034 + 0.0405 \cdot \exp[-0.5(\frac{\log D_g + 1.659}{0.7101})^2] \quad (5.1)$$

Where:

K : Soil erodibility factor (t ha h ha^{-1} MJ^{-1} mm^{-1})
D_g : Geometric mean weight diameter of the primary soil particles (mm)

D_g is a function of surface texture, and its value can be calculated using the method proposed by Torri, Poesen & Borselli (1997):

$$D_g = \exp(\sum f_i \cdot \ln(\sqrt{d_i d_{i-1}})) \quad (5.2)$$

For each particle size class (clay, silt, sand), d_I is the maximum diameter (mm), d_{I-1} is the minimum diameter and f_I is the corresponding mass fraction.

For some soils erodibility is determined largely by soil properties other than texture. This is especially true for volcanic soils. The physical and chemical properties of these soils makes them extremely vulnerable to soil erosion, and the associated erodibility values are beyond the range that is predicted by Equation 5.1 (Torri, personal communication). After careful consideration it was decided to assign an erodibility value of 0.08 t ha h ha^{-1} MJ^{-1} mm^{-1} to all volcanic soils.

5.2 Soil data and processing

Information on soil surface texture was derived from the 1:1,000,000 Soil Geographical Database of Europe (SGDBE, see Heineke *et al.* (1998) for more details). Texture information in the database is stored at the 'soil typological unit' (STU) level. Each soil *mapping* unit (SMU) is made up of one or more STUs. This is shown in Figure 5.1.

For each texture class, 'representative' percentages of clay, silt and sand were estimated based on the class descriptions. The positions of these 'representative'

values in the texture triangle are shown in Figure 5.2. These values were then used to estimate D_g for each texture class. Finally, the erodibility factor (*K*) was estimated using Equation (5.1). Table 5.1 gives an overview of the texture parameters and estimated K-values for each texture class.

For each Soil Mapping Unit (SMU), a K-value was estimated for all its underlying STUs. Then a weighted average was computed, where the weights are proportional to the area of each STU within a SMU. Volcanic soils were treated in a different way: first, all volcanic soils were identified using the parent material code in the soil database. Then, a fixed K-value of 0.08 was assigned to all volcanic soils, irrespective of surface texture. The resulting erodibility map is shown in Figure 5.3.

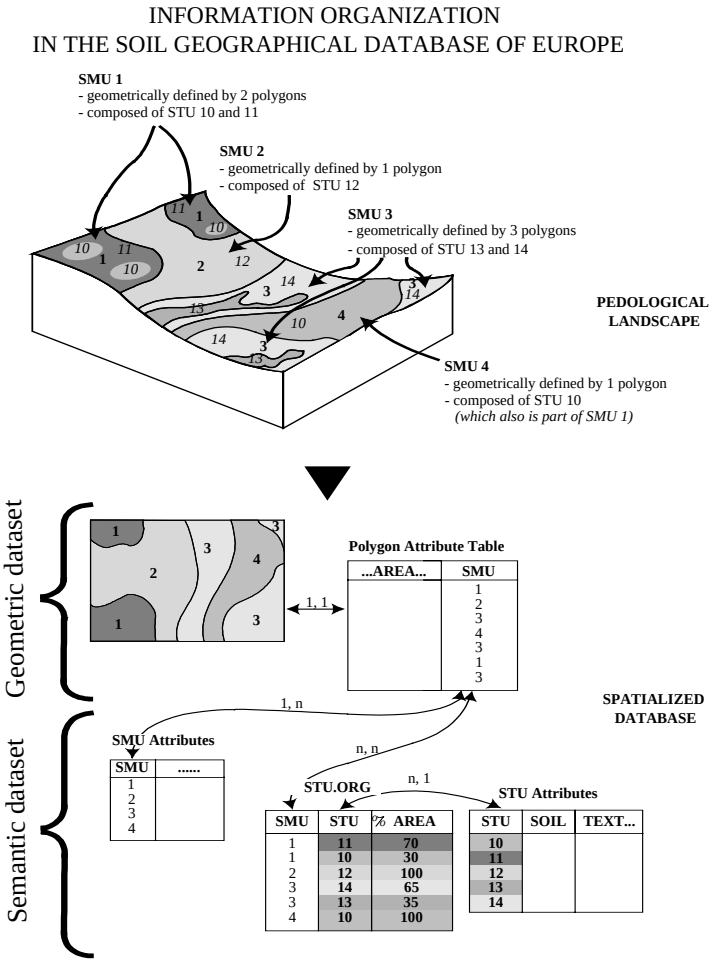

Figure 5.1 *Information organisation in the Soil Geographical Database of Europe.*

Table 5.1 *'Representative' texture parameters for each texture class*

TEXT	Dominant surface textural class.				
	(Present in: STU)	**% clay**	**% silt**	**% sand**	**K**
0	No information	-	-	-	
9	No texture (histosols, ...)	-	-	-	
1	Coarse (clay < 18 % and sand > 65 %)	9	8	83	0.0259
2	Medium (18% < clay < 35% and sand > 15%, or clay < 18% and 15% < sand < 65%)	27	15	58	0.0433
3	Medium fine (clay < 35 % and sand < 15 %)	18	74	8	0.0353
4	Fine (35 % < clay < 60 %)	48	48	4	0.0184
5	Very fine (clay > 60 %)	80	20	0	0.0072

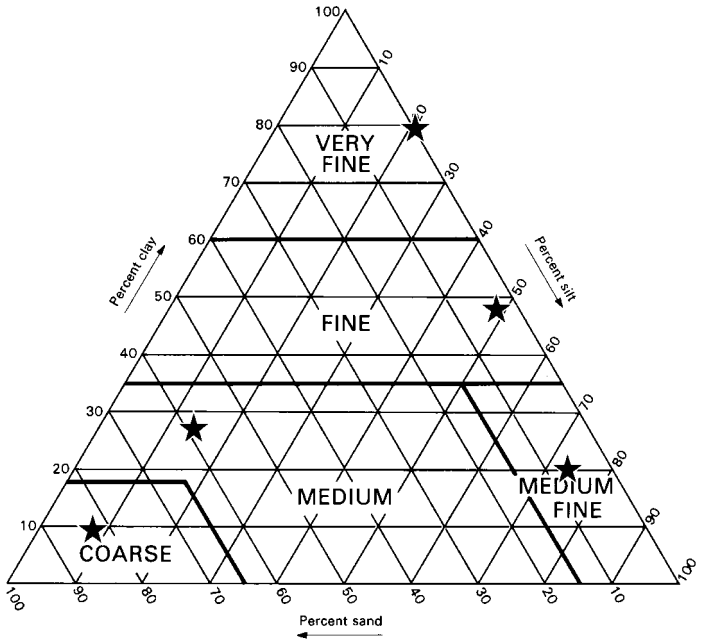

Figure 5.2 *Position of 'representative' texture parameters within the texture triangle*

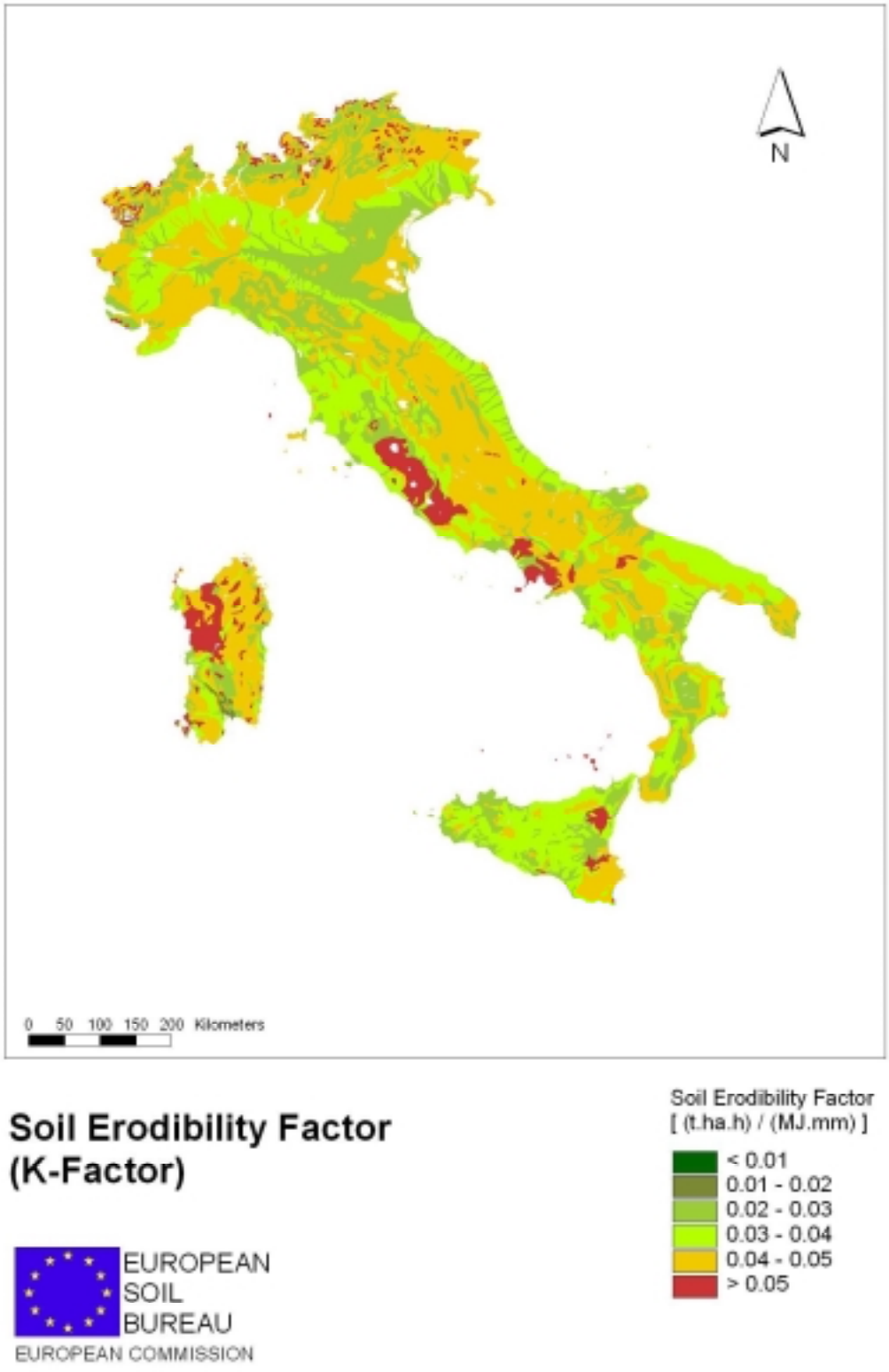

Figure 5.3 *Soil erodibility map (K-factor) (t ha h ha^{-1} MJ^{-1} mm^{-1}).*

6. Cover management factor

6.1 Introduction

Vegetation cover is – after topography – the second most important factor that controls soil erosion risk. In the (Revised) Universal Soil Loss Equation, the effect of vegetation cover is incorporated in the cover management factor (hereafter called C-factor). It is defined as the ratio of soil loss from land cropped under specific conditions to the corresponding loss from clean-tilled, continuous fallow (Wischmeier & Smith, 1978). The value of C mainly depends on the vegetation's cover percentage and growth stage. The effect of mulch cover, crop residues and tillage operations should also be accounted for in the C-factor. In the Revised Universal Soil Loss Equation (Renard *et al.*, 1997) the C-factor is subdivided into 5 separate sub-factors that account for the effects of prior land use, canopy cover, surface cover, surface roughness and soil moisture respectively. At the national scale, it is hardly possible to estimate C using the RUSLE guidelines due to a lack of sufficiently detailed data. Moreover, some additional problems arise when the model is applied at a national scale.

Up to the regional scale it would be fairly easy to assign monthly C-values to classes in the CORINE land cover database by means of a lookup-table. However, at the scale used here this approach would be problematic, as Italy encompasses a wide variety of climatic conditions, which results in large spatial and temporal variations in growing season and crop vigour. This would be extremely difficult to incorporate using a table-based approach.

Instead, NOAA AVHRR imagery was used to obtain approximate C-factor values.

6.2 NOAA AVHRR

AVHRR is an acronym for 'Advanced Very High Resolution Radiometer'. It is a four (AVHRR/1) or five (AVHRR/2) channel radiometer with channels in the visible, near infrared, middle infrared and far infrared parts of the electromagnetic spectrum (http://www.belspo.be/telsat/avhrr/avts_001.htm). It has a ground resolution of approximately 1.1 km. The satellite orbits the earth 14 times each day, resulting in a daily global (pole-to pole) coverage. An automatic algorithm is used to geometrically correct the images, resulting in a geometric accuracy of about 4 km.

6.3 Normalised-Difference Vegetation Index

The most widely used remote-sensing derived indicator of vegetation growth is the Normalised Difference Vegetation Index (NDVI):

$$NDVI = \frac{(AVHRR2 - AVHRR1)}{(AVHRR2 + AVHRR1)}$$

Where:

AVHRR1 : Reflectance value Channel 1 (visible)
AVHRR2 : Reflectance value Channel 2 (near infrared)

Its value varies between –1 and 1, where low values can be found at water bodies, bare soil and built-up areas. NDVI is positively correlated with the amount of green biomass, so it can be used to give an indication for differences in green vegetation cover.

6.4 Correlations between NDVI and vegetation properties

De Jong (1994) investigated the use of LANDSAT Thematic Mapper (TM) imagery for deriving vegetation properties like Leaf Area Index (LAI), percentage cover and the USLE-C factor. For this, areal estimates of percentage cover, LAI and C were obtained from 33 plots in the Ardêche province in France. The plot values were compared with the corresponding NDVI-values on the TM-image (local average of a 150 by 150 m window around the plot location), yielding regression equations that are able to predict LAI, percentage cover and USLE-C from NDVI-values. Using a linear model he found a correlation between NDVI and USLE-C of –0.64. According to De Jong, the somewhat poor results could possibly be explained by the sensitivity of the NDVI for the vitality of the vegetation: for a canopy under (water) stress NDVI will be low, even if the canopy cover is dense. This seriously limits the use of NDVI images in erosion studies, because for erosion the condition of the vegetation is not important.

6.5 NDVI profiles

In order to get a better picture of the usefulness of NDVI images, NDVI ‘profiles’ were created for various land cover classes. First, a series of daily NDVI-images of 1998 was obtained for the whole of Italy. To reduce the influence of cloud pixels, 36 composite images were created which contain –for each pixel– the maximum NDVI value of 10 days. The CORINE landcover database was re-projected to the same co-ordinate system as the NDVI-images, so that both could be overlain. For six major CORINE landcover classes sample pixels were digitised. Because of the geometric accuracy of the NDVI-images (around 4 km), for each class only pixels were selected that are near the centre of large contiguous areas of the same CORINE class. This way, the risk of ‘mixed’ pixels is minimised. It should be stressed that this implicitly assumes that the CORINE landcover class presents the actual landcover (e.g. that CORINE is ‘correct’), which is not necessarily the case. The locations of the profiles are shown in Figure 6.1.

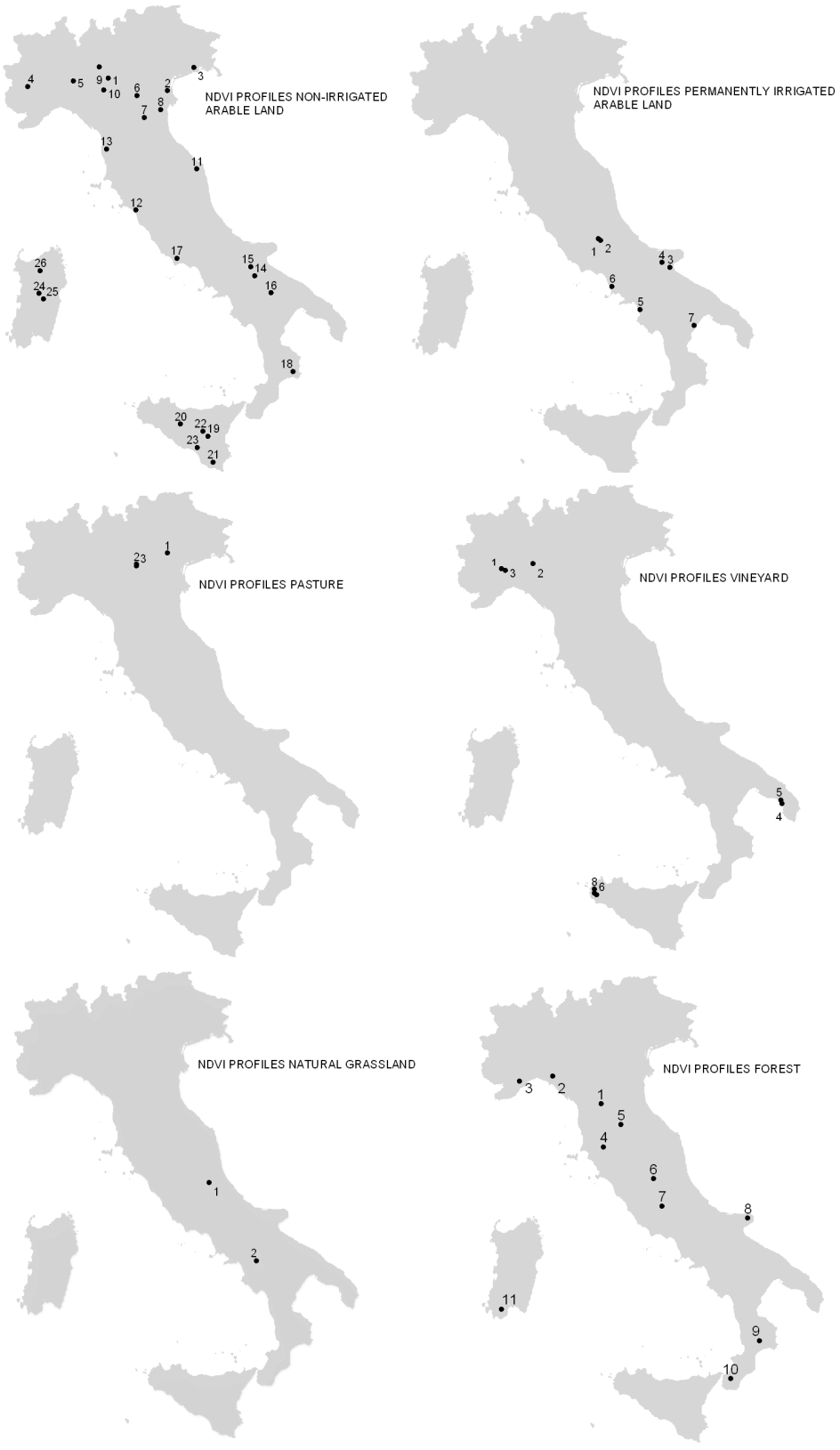

Figure 6.1 *Locations of the NDVI profiles*

The 10-daily NDVI composites were smoothed by taking for each pixel the local average NDVI value within a 4km x 4km square neighbourhood. For each sample pixel, yearly timeseries of these smoothed NDVI values were created. Some typical results are shown in Figure 6.2 (note that these graphs actually show the NDVI values multiplied by 200, while negative values are truncated to zero). From the profiles some interesting trends can be observed.

First, the arable land classes clearly show crop senescence and decline over the year. The time at which maximum NDVI is reached ranges between the end of July for the north to mid-April for Sicily. Thus, the profiles reflect a shift in the growing season when moving from north to south. This shows that simply assigning USLE-C values to entire landcover classes would not give a very accurate approximation of vegetation growth and decline over the year.

Second, the NDVI response for pasture is fairly constant over the year, which is in agreement with the expected pattern. Noteworthy is the high variability of the NDVI response of forest, often showing very low values in winter. For the vineyard profiles, it is interesting to note that the NDVI response is generally lower in the south than in the north. This may indicate that the southern vineyards are –in terms of biomass production– either less productive or that they are simply subject to more water stress. Due to a lack of large, contiguous areas of natural grassland, only one profile could be constructed. The response is similar to pasture, although the NDVI-values are generally lower.

Of course, the observations made here should be viewed with some caution: for some classes the number of profiles is quite small so they are not necessarily ‘representative’. Also, taking into account the pixel size and geometric accuracy of the NDVI images as well as the generalisation used in the CORINE database, pixels may be ‘mixed’, therefore not representing a ‘typical’ NDVI-response for their respective CORINE class.

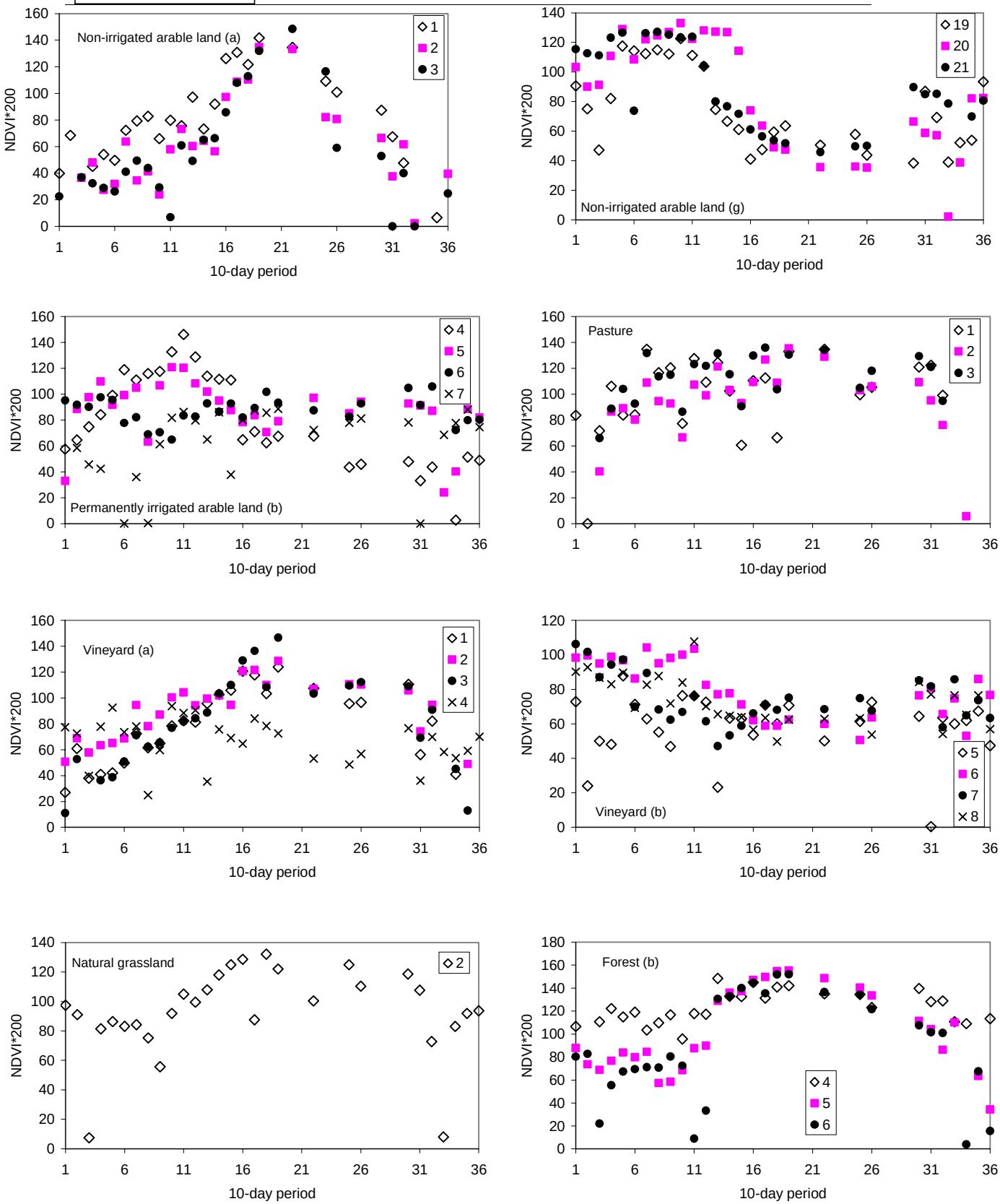

Figure 6.2 *NDVI profiles for various CORINE landcover classes*

6.6 Estimating the USLE-C factor from NDVI values

De Jong (1994) derived the following function for estimating USLE-C from NDVI (revised in De Jong *et al.*, 1998):

$$C = 0.431 - 0.805 \cdot NDVI \qquad (6.1)$$

The function has a correlation coefficient of –0.64, which is modest but nevertheless significant. The function was tested on several NDVI profiles. In general, estimated C-values were found to be rather low. Furthermore, De Jong's equation is unable to predict C-values over 0.431. Also, the function was obtained for (semi-)natural vegetation types only, using Landsat TM imagery whose spectral and geometric characteristics are quite different from the NOAA images used here. Because of these problems, it was investigated whether the NDVI-images could be 'scaled' to approximate USLE-C values in some alternative way. After some experimentation, the following provisional equation seemed adequate:

$$C = \exp\left[-\alpha \cdot \frac{NDVI}{(\beta - NDVI)}\right] \qquad (6.2)$$

Where:

α, β : Parameters that determine the shape of the NDVI-C curve

An α-value of 2 and a β-value of 1 seem to give reasonable results. Figure 6.3 shows the corresponding (hypothetical) relationship between NDVI and C.

It should be emphasised that, at this stage, no field data are available that justify the use of Equation 6.2. However, the equation seems to produce more realistic C values than those estimated assuming a linear relationship. The proposed values for α and β were obtained by 'calibrating' Equation 6.2 on the NDVI-profiles described in Section 6.5. The scaling constants in Equation 7 were then adjusted until reasonable monthly C-values were obtained.

Some typical results are shown in Figure 6.4. Note that the C-values in the figure are running means of three 10-day periods:

$$C_{av} = \frac{1}{3} \cdot (C_{t-1} + C_t + C_{t+1}) \qquad (6.3)$$

Several trends are apparent in Figure 6.4. For most of the year, the estimated C-values for pasture seem rather high when compared to published literature values. Predicted C-values for forest are near zero for most of the summer, which looks realistic. However, especially the winter values seem unrealistically high. The most likely explanation for this is that the NDVI is only sensitive for healthy, photosynthetically active vegetation. Forests usually have a thick mulch layer which provides excellent protection against soil erosion. Unfortunately, mulches cannot be detected on NDVI-imagery.

The predicted C-values of the arable classes are more difficult to judge, because the actual C-values mainly depend on crop type and management practices, both of which are unknown in this case. The range of predicted values looks fairly realistic, although the winter values seem quite low. This may be explained by the large pixel size and the coarse geometric accuracy of the images, which may 'average out' extreme NDVI-values.

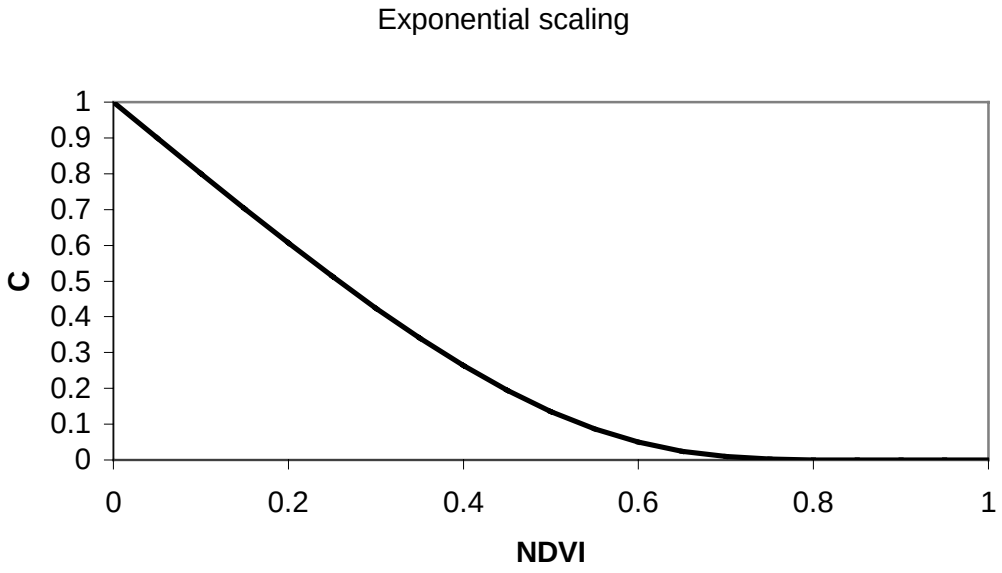

Figure 6.3 *Relationship between NDVI and USLE-C according to exponential scaling formula*

The results for the profile locations show that the NDVI images can be used only to obtain very rough approximations of the USLE-C factor. Monthly C-maps for the whole of Italy were created following a five-step procedure:

1. The 10-daily images are aggregated into monthly images by taking, for each pixel, the average NDVI value for 3 succeeding images. In case of 'missing data' pixels in one of the 10-daily images, the average for the remaining image(s) is used.
2. 'Missing data' pixels in the monthly images are replaced by the average NDVI of the corresponding pixels in the preceding and succeeding monthly image, i.e.:

$$NDVI_t = \frac{(NDVI_{(t-1)} + NDVI_{(t+1)})}{2} \qquad (6.4)$$

3. The monthly images are transformed to the 'Lambert Equal Area'-projection that is also used for the remainder of the dataset.
4. Equation 6.2 is used to obtain pixel-by-pixel estimates of C.

5. For a number of land cover classes in the CORINE landcover database, maximum C-values are defined. This is done mainly to prevent unrealistically high winter values for woodland and pasture. The maximum values used are 0.01 for woodland and pasture and 0.05 for natural grassland.

USLE-C maps (aggregated by season) are shown in Figure 6.5.

6.7 Discussion and conclusions

The analysis of the NDVI-profiles shows that NDVI-images can be used only for giving a rough approximation of the USLE-C factor. However, relying solely on the NDVI-values will produce erroneous results in cases where soil cover is made up of decaying biomass, like humus layers, mulches or other dead organic material. This especially results in unrealistically high winter C-values for woodland. Theoretically, land-use specific upper- and lower C-values could be assigned to CORINE landcover classes. This has been done for woodland, grassland and pasture, although it is not really appropriate due to the rather coarse geometric accuracy of the NDVI-images (4km x 4km).

The approach followed here will result in very rough estimates of the C-factor. In spite of all its shortcomings though, it may be the best information that can be obtained using the available data. To improve the results, imagery with better geometric and spectral characteristics are needed, as well as more field measurements that can be used to relate biophysical properties (like the C-factor) to remotely-sensed data.

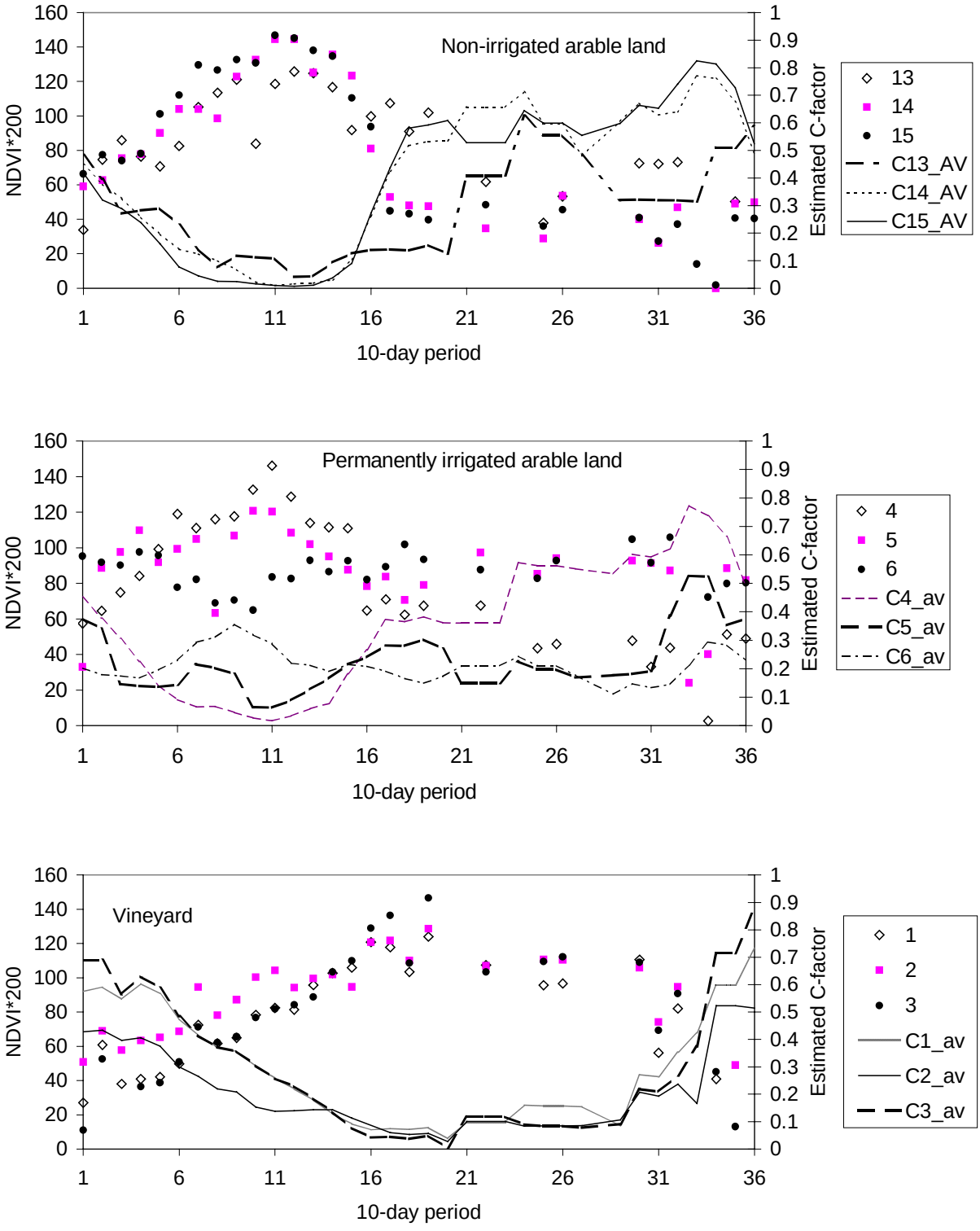

Figure 6.4a *NDVI-derived USLE-C values for some CORINE classes.*

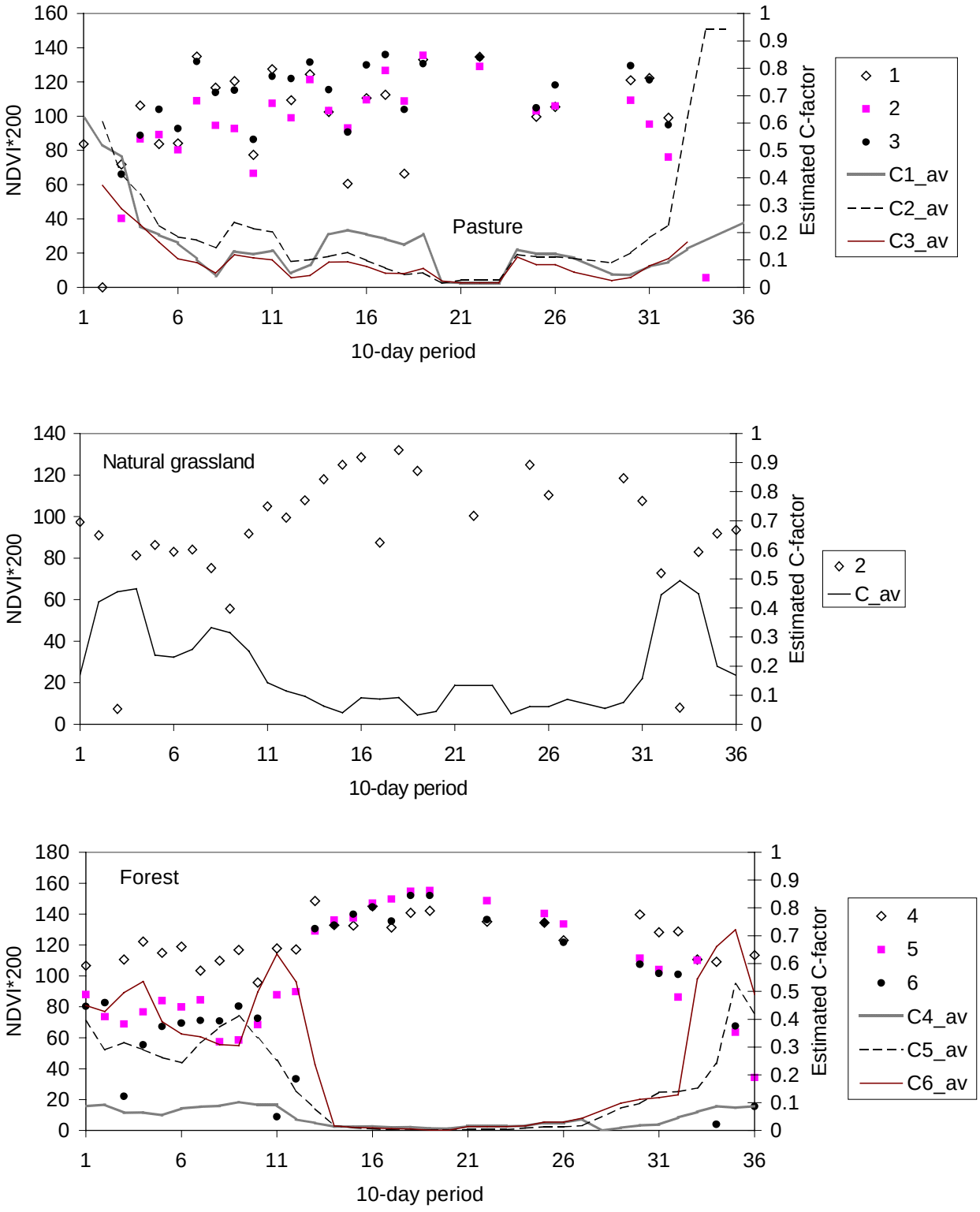

Figure 6.4b *NDVI-derived USLE-C values for some CORINE classes.*

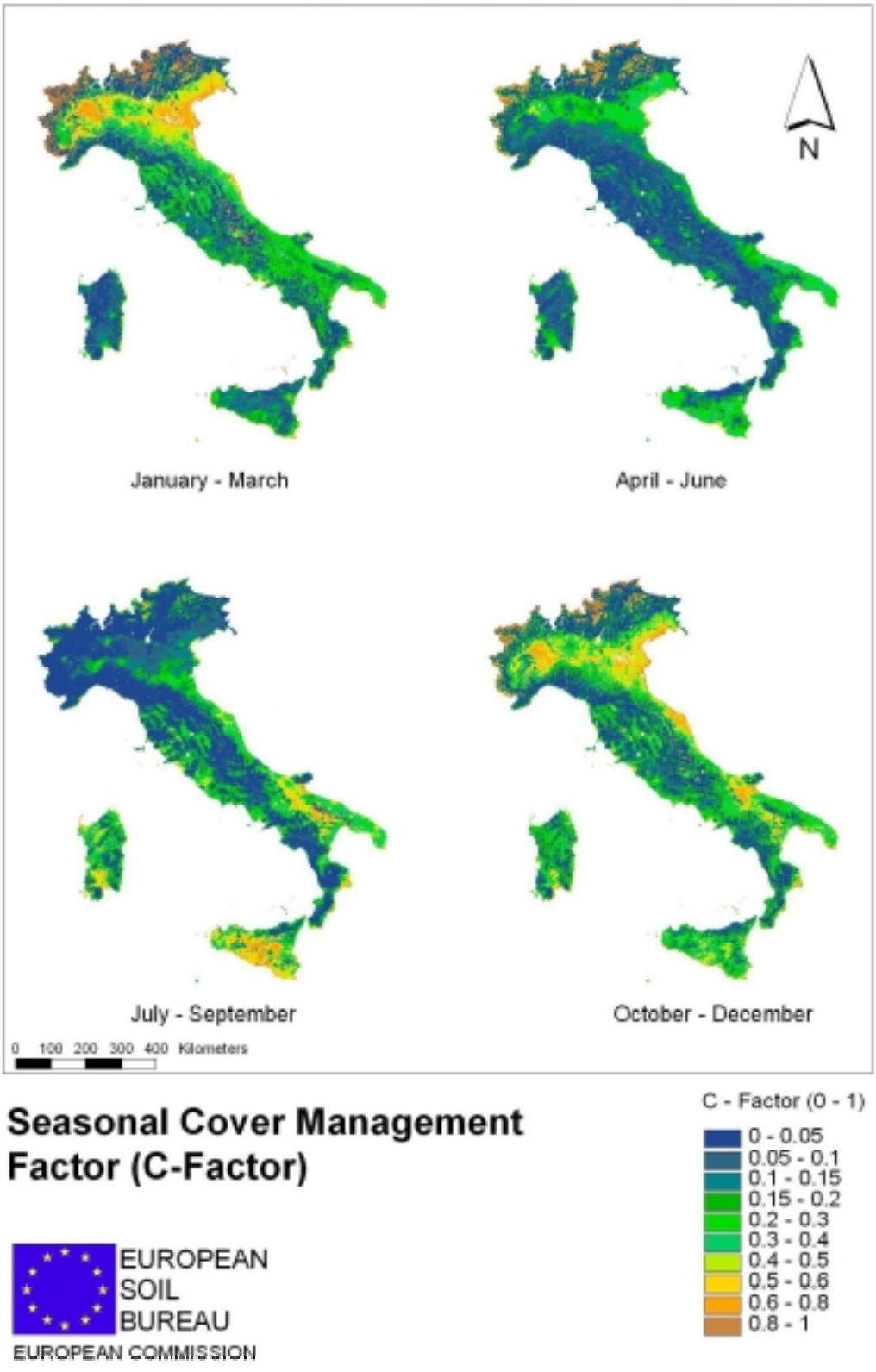

Figure 6.5 *Seasonal cover management factor maps (C-factor) (dimensionless).*

7. Slope- and slope length factors

The slope- and slope length factors were estimated using the equations of Moore *et al.* (1993):

$$L = 1.4(\frac{A_s}{22.13})^{0.4} \quad (7.1)$$

$$S = (\frac{\sin \beta}{0.0896})^{1.3} \quad (7.2)$$

Where:

A_s : Specific contributing area (m^2/m)
β : Slope angle (degrees)

The equations of Moore *et al.* have the advantage over the 'original' equations by Wischmeier & Smith (1978) that they use specific contributing area as a slope length estimate, which is more amenable to three-dimensional landscapes.

Slope was calculated using a 250-metre resolution digital elevation model (DEM) of Italy. Estimating specific contributing area proved to be difficult using the 250-m DEM, because its value would always be greater than or equal to 250 metres, which is rather high when compared to the range of slope lengths for which the USLE was originally developed. Therefore, a constant A_s value of 50 metres was assumed. This value is completely arbitrary, and it is by no means representative or 'typical' for Italian conditions. The use of a more detailed DEM (50-m resolution or better) could provide better estimates of the slope length factor.

Figure 7.1 shows the resulting LS map.

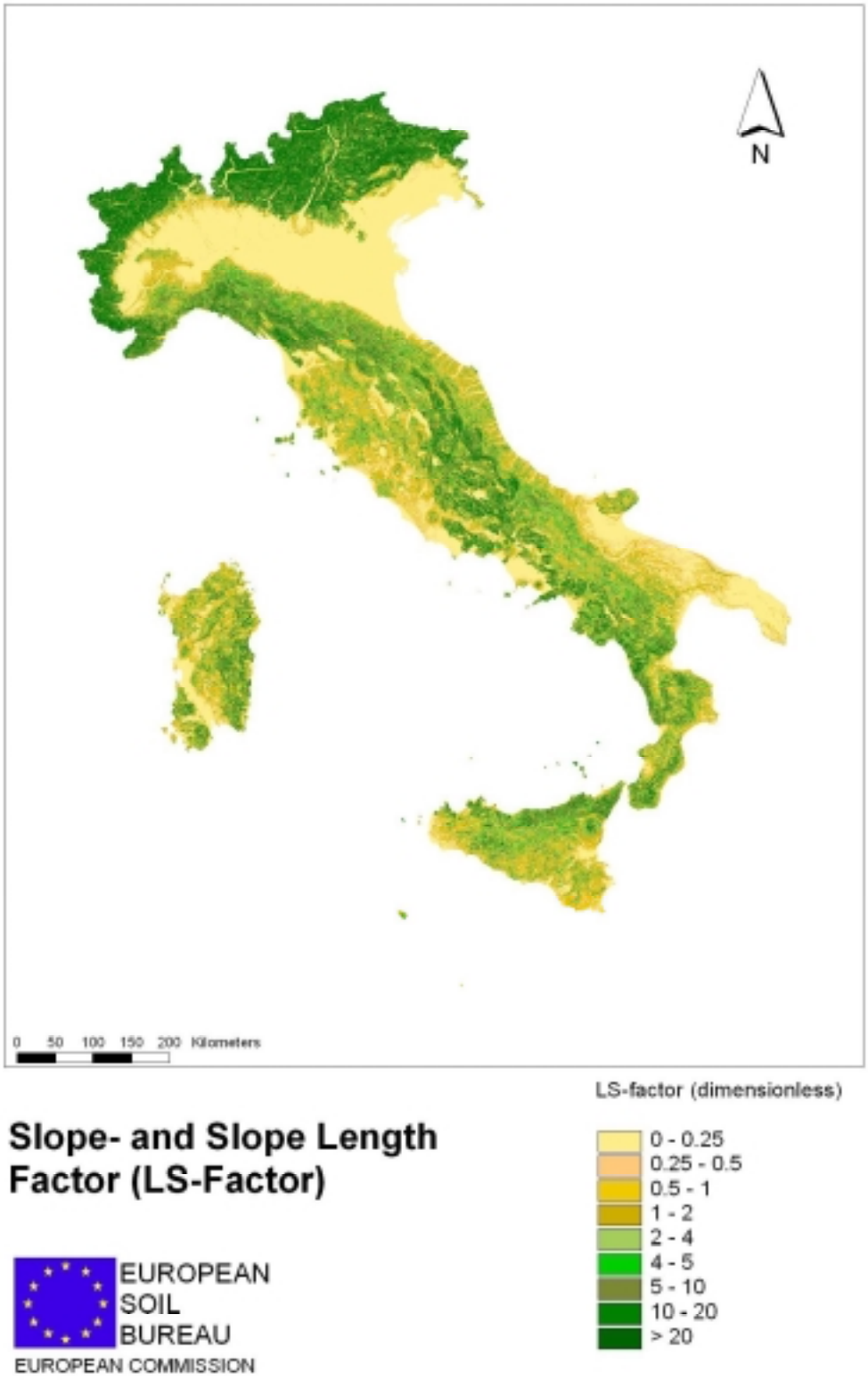

Figure 7.1 *Slope / Slope length factor map (LS) (dimensionless)*.

8. Results and discussion

8.1 Results

The previous chapters described the derivation of the various factors of the USLE. The USLE was run with a monthly time interval. This way, the annual variation in rainfall and vegetation growth is taken into account, as is the interaction between the two. The model output consists of monthly erosion risk maps, which are shown in Figure 8.1.

An estimate of actual annual soil erosion risk is shown in Figure 8.2. Figure 8.2a is a generalised erosion map for the whole of Italy. To improve its visual appearance, the map was smoothed using a median filter that replaces the actual pixel values by the median of all pixel values within a 1.3-km search radius. Figure 8.2b shows a more detailed (unsmoothed) map of Sicily, and central Italy is shown in more detail in Figure 8.2c. *Potential* erosion risk was assessed by running the USLE on the assumption that there is a total absence of vegetative cover (i.e. $C = 1$). The resulting potential erosion risk map is shown in Figure 8.3.

It is also possible to aggregate the predicted erosion figures by administrative boundaries. Figure 8.4 shows erosion risk by province. the map was produced by computing, for each province, the median predicted erosion rate. Similarly, Figure 8.5 shows erosion risk aggregated by community. It must be noted here that the erosion pattern as shown on these maps depends heavily on the size and shape of the regions that are used to aggregate the results.

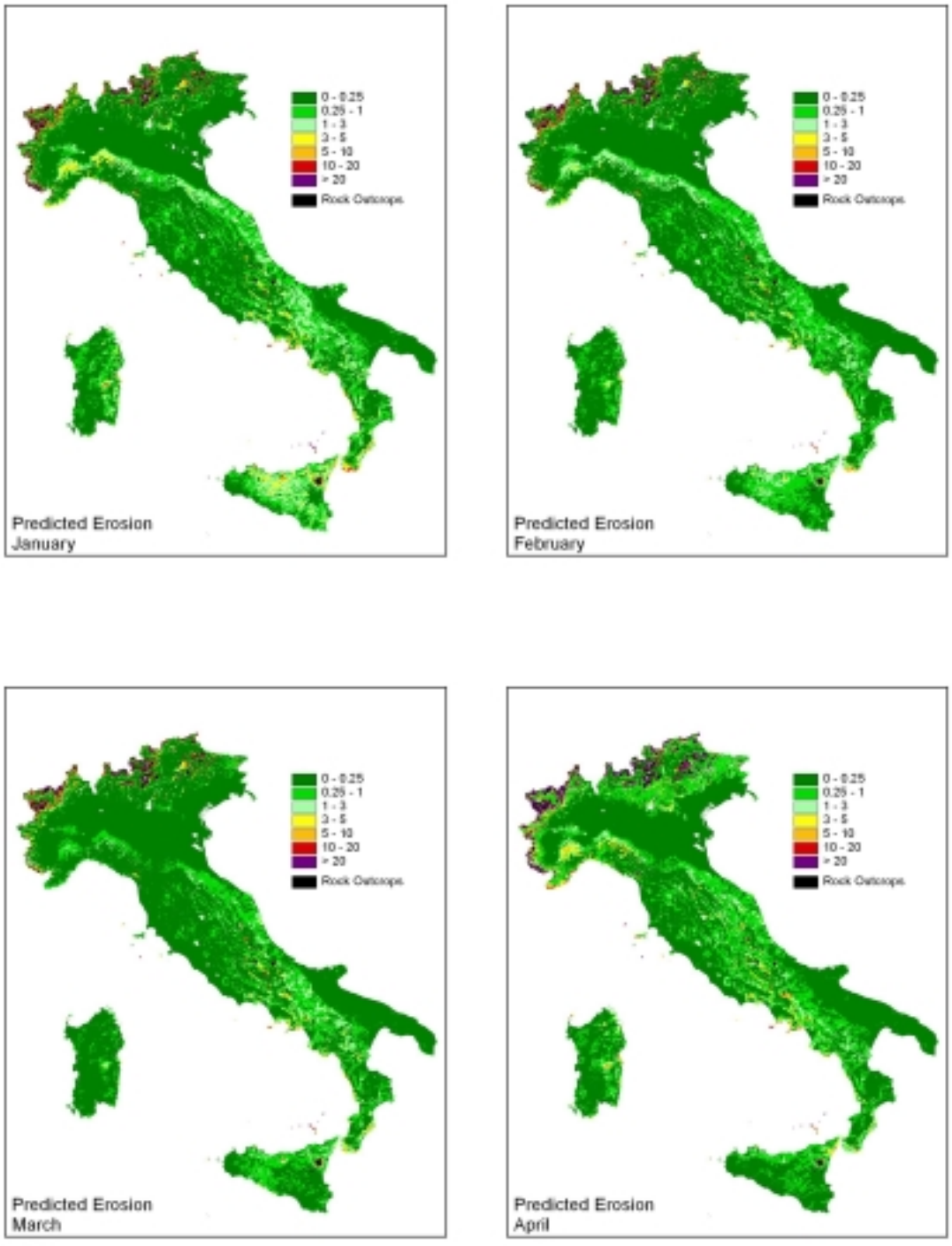

Figure 8.1a *Predicted erosion by month*

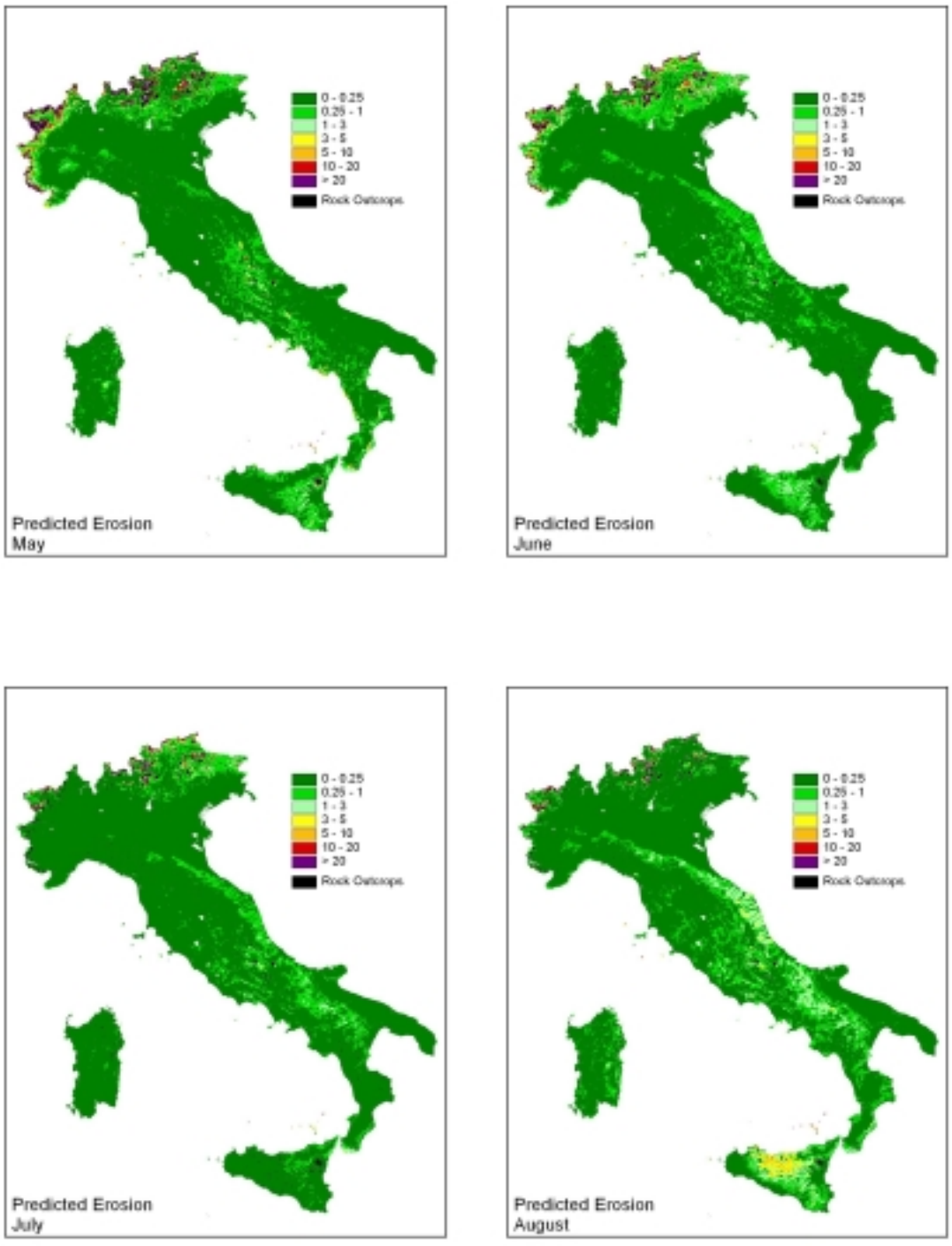

Figure 8.1b *Predicted erosion by month*

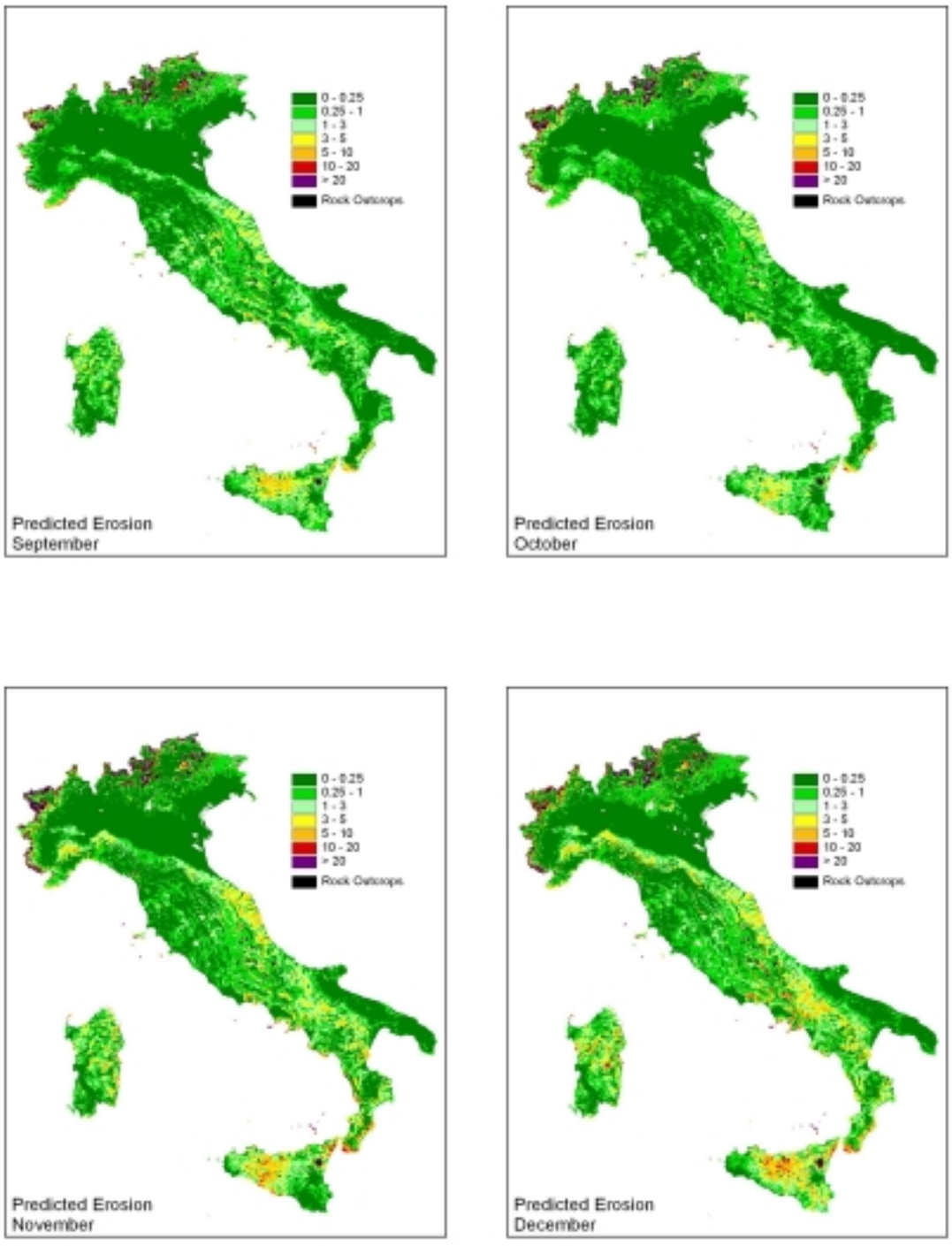

Figure 8.1c *Predicted erosion by month*

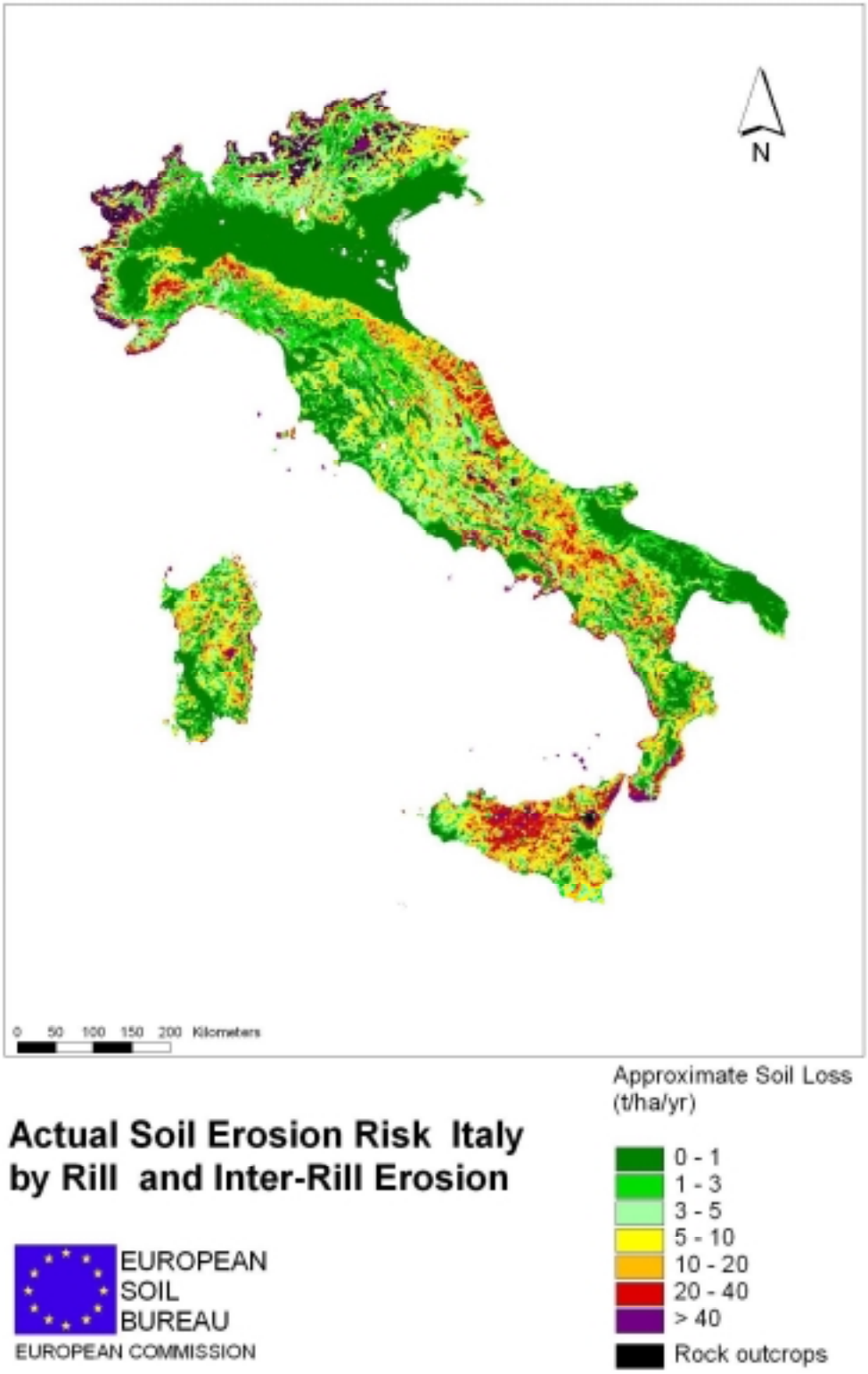

Figure 8.2a *Soil erosion risk map of Italy: Actual erosion risk.*

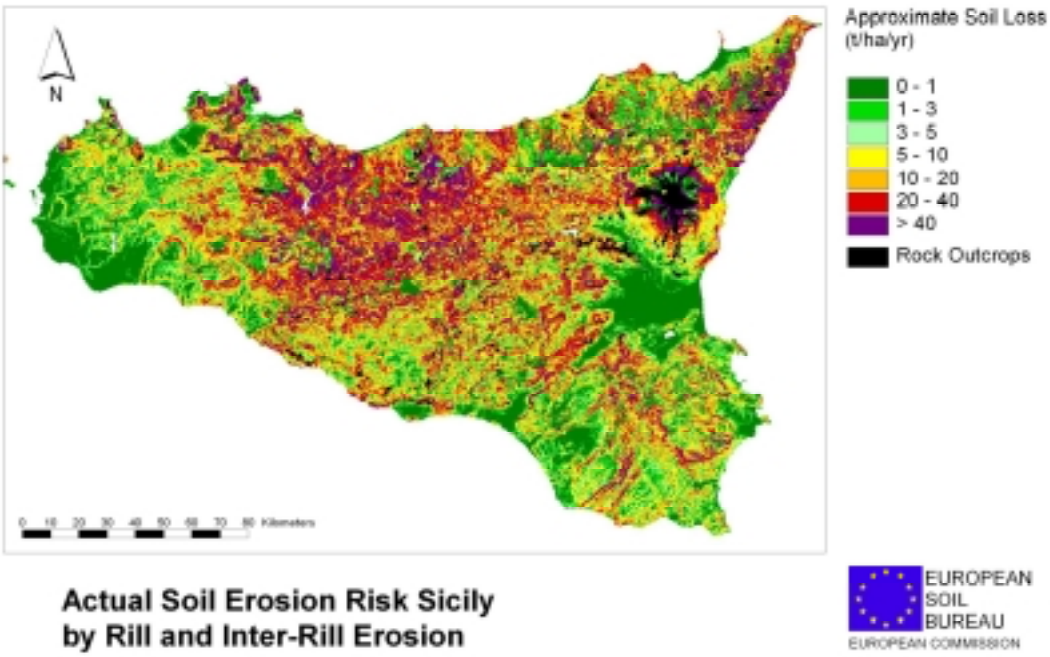

Figure 8.2b *Soil erosion risk map of Italy: Actual erosion risk Sicily.*

Figure 8.2c*Soil erosion risk map of Italy: Actual erosion risk central Italy.*

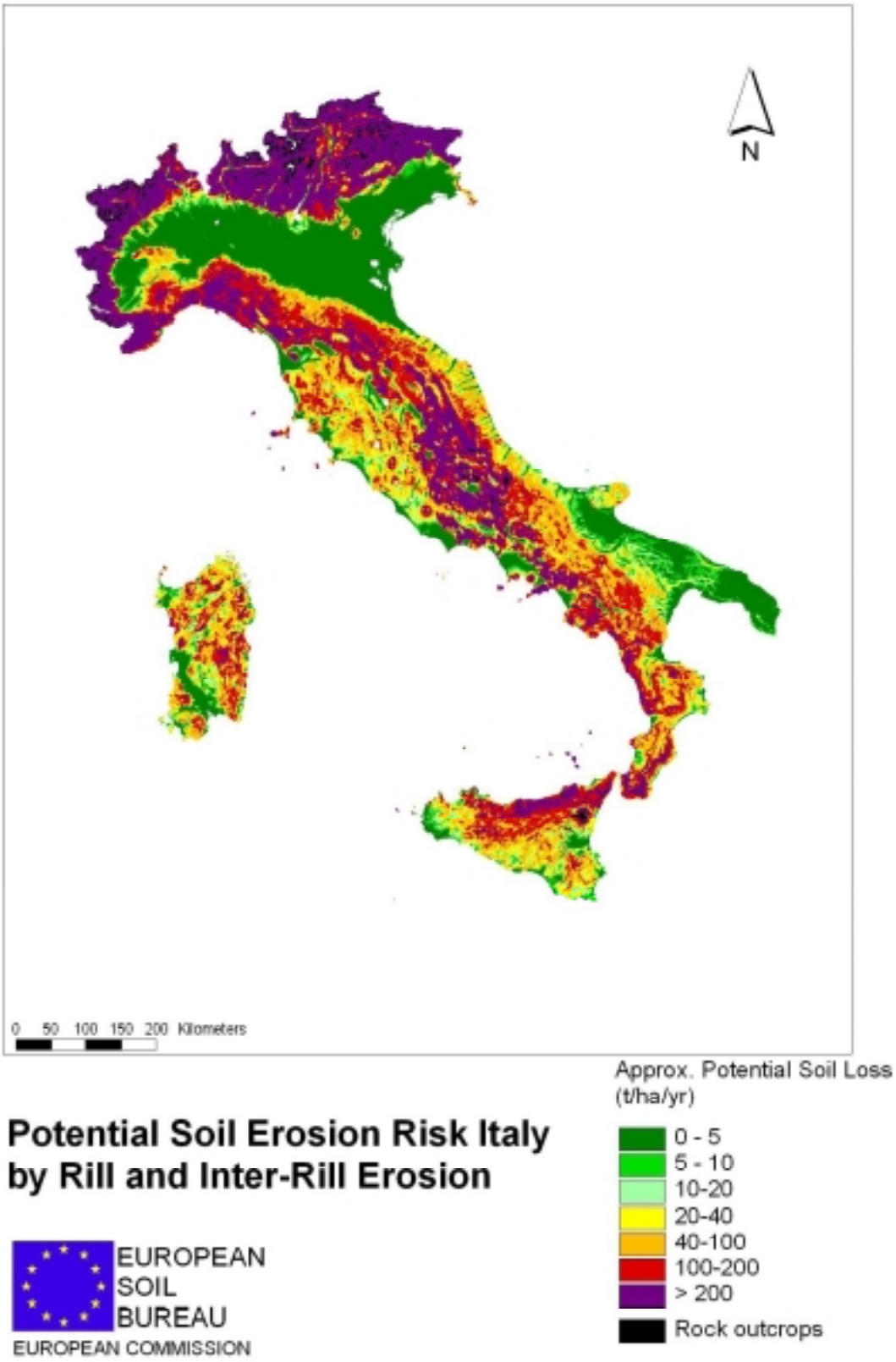

Figure 8.3 *Potential soil erosion risk.*

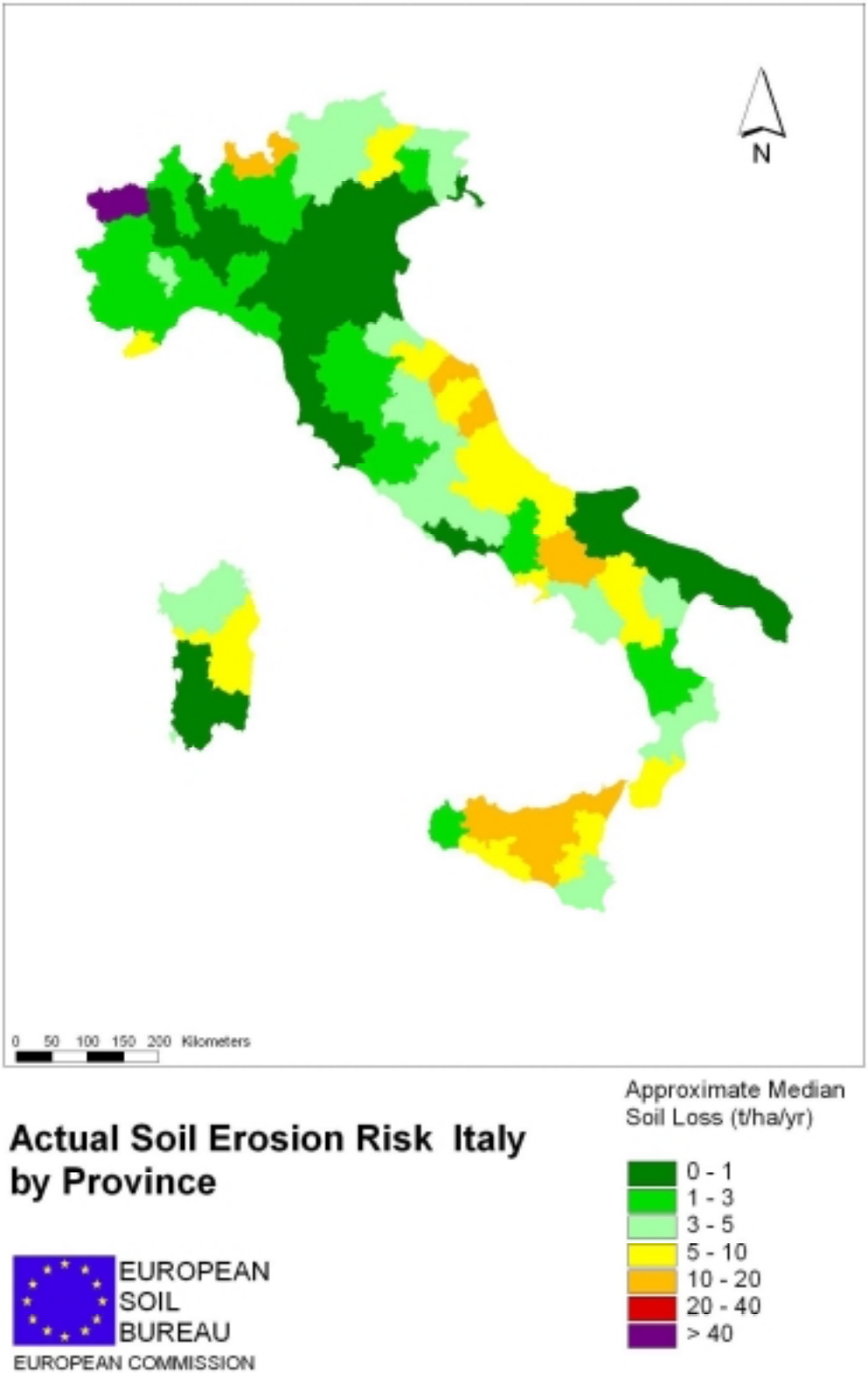

Figure 8.4 *Soil erosion risk by province.*

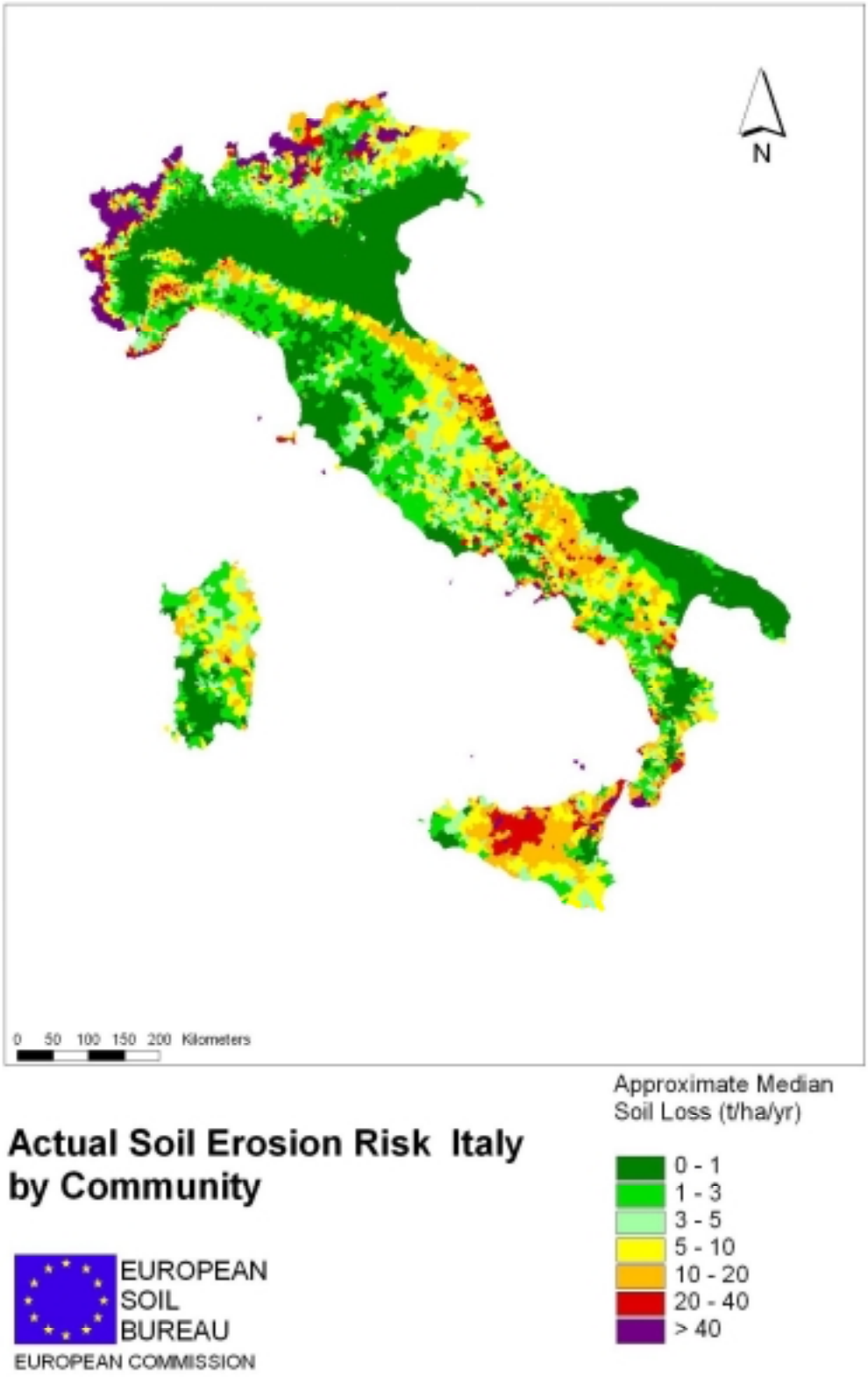

Figure 8.5 *Soil erosion risk by community.*

8.2 Discussion

A proper validation of the results is hardly possible at the scale used. Nevertheless, it is possible to make some comments on the general pattern of the map for some areas.

First, the erosion rates on the map seem quite low for large parts of Tuscany (Torri, pers. comm.). This is partly because the main type of erosion here is gully erosion, which cannot be predicted using the USLE-based approach used (possibly unless a very detailed digital elevation model is available). Also, erosion is often related to geology here: the presence of joints in the bedrock material can lead to the development of pipes and gullies, which is not taken into account.

Another reason for the overall low erosion rates is the NDVI-derived C-factor value, which is underestimated in some cases. For example, in the Chianti area all the cultivated fields are bare from July to December, and C should be varying between 0.5-0.8 in summer-autumn period. The NDVI-derived values for this period are around 0.2-0.4, which is much lower. A possible explanation may be the 1-km pixel size of the NOAA imagery which causes NDVI-response to be averaged out over large areas. Even though a large proportion of the area is bare during this period, there are small patches of very dense maquis/garrigue like vegetation that would be expected to show a much higher NDVI-response. Consequently, the NDVI response of each 1-km pixel contains a mixed signal, from which it is difficult to obtain sensible *C*-values. The fact that a highly non-linear equation is used to estimate *C* complicates things further, as it makes up-scaling less straightforward. This can be demonstrated using a simple example.

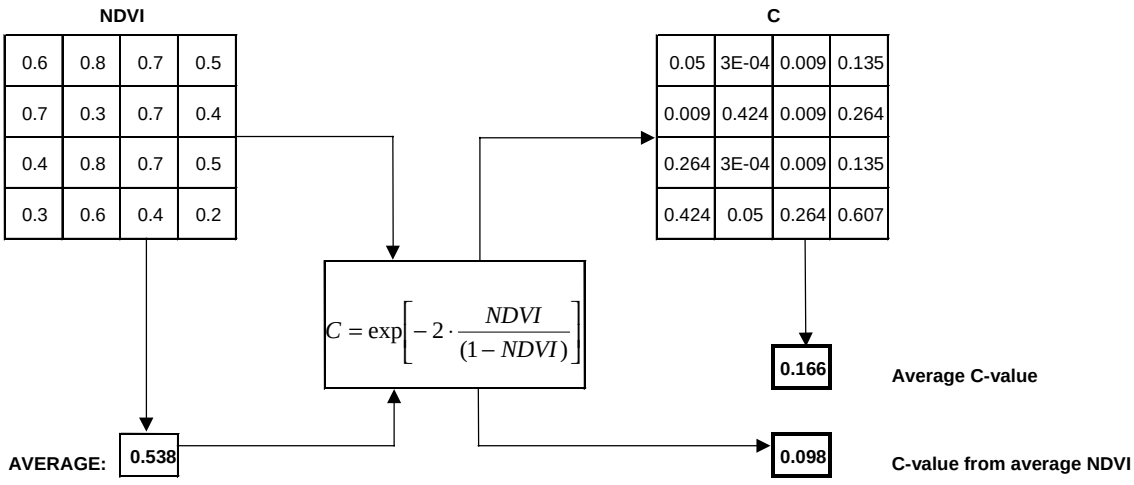

Figure 8.6 *Effect of pixel size on predicted C-values (See text for explanation)*.

Figure 8.6 shows a 4 by 4 cell grid of NDVI-values. Average NDVI is 0.538. For each pixel, an estimate of C is obtained using Equation 6.2 (for the sake of simplicity, it is

assumed here that this will result in a 'correct' estimate of *C*). The average *C*-value is 0.166. Applying Equation 6.2 directly on the average NDVI-value (the entire grid is now treated as a single pixel) results in a predicted 'average' *C*-value that is about 40% lower. This example demonstrates the dependence of predicted C-value on cell size, and it shows that the predicted *C* values may be biased if sub-pixel information is not known.

Second, erosion seems to be overestimated in areas with stepped relief (Torri, pers. comm.). For example, there is an area in Umbria where the slopes are made up of nearly flat plateaux separated by much steeper parts, resulting in a stepped relief. Erosion on the plateaux is close to nil. The 250-m elevation model used to derive slopes is too coarse too distinguish the steps, leading to slope estimates that are generally too high. Hence, erosion seems to be overestimated in these areas. It should be emphasised though that this is a special case, as the 250-m resolution DEM generally results in slope estimates that are too low.

Apart from the problems mentioned above, it should be stressed here that the results of the spatial analyses presented here have many other limitations and shortcomings. First of all, the Universal Soil Loss Equation only gives a very crude estimate of long-term expected soil loss. It only predicts rill- and interrill erosion: gully erosion is not taken into account (although it could be included if a sufficiently detailed elevation model would be available). Deposition is not included, only gross erosion is predicted. As long as any of the factors in the equation is greater than zero, some erosion will be predicted, even if the actual erosion is nil. Some authors claim that it is possible to identify areas where deposition will occur using very detailed elevation models (Moore & Burch, 1986; Mitasova *et al.*, 1996), although this is still a matter of controversy.

Furthermore, some important factors influencing soil erosion are not taken into consideration. First, the effect of stones and rock fragments in the soil is not included. Römkens (1985) suggests that the effect of stones is best considered in the *C*-factor of the USLE, because stones protect the soil surface in a similar way as a surface mulch. Although the European Soil Geographical Database provides a way to estimate stone volume through a pedotransfer rule (Daroussin & King, 1996), only two stone volume classes are distinguished which is too crude for assessing erosion risk.

Second, the effect of management practice is not included in the model. This includes practices such as of contouring, stripcropping, terracing and subsurface drainage (Renard *et al.*, 1997). Although these operations can be included in a so-called 'support practice factor' (P-factor), the effect of management practice is nearly impossible to assess at the scale used here. However, it should be realised that management practice may be one of the most important factors affecting erosion in many cases. Third, erosion by melting snow is not taken into account, even though this may be important in mountainous areas.

Probably even more important than the problems mentioned above are the uncertainties associated with the various data sources. Some of the main sources of uncertainty are:

- The estimate of the rainfall erosivity factor (R), which is based on an approximate relationship with annual rainfall that was established for Tuscany. Extrapolating this 'Tuscan equation' to the whole of Italy is potentially inappropriate because of the wide variety of climatic conditions that are found in Italy, leading to significant deviations from Tuscan conditions.
- The soil erodibility factor (*K*) is estimated from surface texture (except in the case of volcanic soils). However, the actual correlation between K and the texture parameters is rather weak. Moreover, the soil units in the Soil Geographical Database of Europe have an unknown (but probably large) within-unit variance.
- For the LS factor, slope angle was derived from an elevation model with a resolution of 250 metres, which is rather coarse for erosion modelling. Because it was not considered feasible to estimate slope length (or specific contributing area) from the current DEM, an arbitrary constant slope length value was assumed, so in effect slope length is not taken into account.
- The C-factor was estimated using a rather arbitrary scaling procedure of monthly NDVI-images. Because of this, the resulting C-factor values are rather crude estimates.

These and many other uncertainties propagate throughout the model, resulting in an uncertainty in the estimated erosion rate. In theory it is possible to quantify this uncertainty, using either an analytical approach or Monte Carlo simulation (Burrough & McDonnell, 1998). In practice, it is hard to make even crude estimates of the errors associated with each of the individual factors in the USLE. Also, some of the individual factors are interdependent, which results in an even greater impact on the model results.

Despite these deficiencies and shortcomings, the methods outlined in this report have produced valuable information on soil erosion risk. The main value of the spatial analysis is to identify areas that –in the long term– are likely to experience rill- and inter-rill erosion risk. Then, a more detailed assessment may be performed for these areas using more detailed data, more sophisticated erosion models and field surveys. This study is a first attempt to produce a map of soil erosion risk for the whole of Italy. Its value lies in the fact that the estimates of erosion risk are based on standardised, harmonised data sets for the whole country. The interpretation of the maps is complicated by the fact that Italy encompasses a variety of hydrologic regimes, between which the processes influencing soil erosion by water are essentially different. Furthermore, a scientifically sound validation of the results is extremely difficult at this scale.

It should be emphasised that these results should be used with caution. For example, it would not be advised to use the maps to predict soil losses on agricultural parcels or to predict soil loss for any individual year. Only soil erosion by water flow is taken into account, and then only rill- and inter-rill erosion, thus, the maps should not be used to predict the occurrence of mass movements such as landslides and mudflows.

In conclusion, the current soil erosion risk map of Italy may –within the limitations outlined above– simply be close to the best that can be obtained with the available data. The results could be improved by using a more detailed digital elevation model, satellite data that have better spectral and geometric characteristics than the NOAA

AVHRR data that are currently used, more detailed soil information (especially texture and soil depth) and the inclusion of rainfall data from more meteorological stations.

Acknowledgements

The authors are grateful to the following people. Dr. Dino Torri (Istituto per la Genesi e l'Ecologia del Suolo, CNR Firenze) is thanked for his willingness to discuss an earlier draft of the work. Much of Chapter 8 is based on a discussion with him on a preliminary version of the work, which has benefited considerably from his comments, criticism and suggestions. Dr. Camillo Zanchi (Univ. Firenze, Dip. di Agronomia) is thanked for providing some unpublished results of his research on rainfall erosivity in Tuscany. Dr. Ad De Roo (JRC-Ispra) is thanked for the useful discussions on erosion modelling and for his comments on the analyses. Giorgio Passera (JRC Ispra) is thanked for preparing the 10-daily NDVI-composites. The example shown in Figure 8.6 was inspired by an e-mail from Dr. Raimon Salvador (CREAF, Universitat Autonoma de Barcelona). This study was financed by the Italian Ministry of Agriculture.

References

Arnoldus, H.M.J. (1978). An approximation of the rainfall factor in the Universal Soil Loss Equation. In: De Boodt, M. & Gabriels, D. (eds): *Assessment of erosion*, p. 127-132. Wiley, Chichester.

Burrough, P.A. and McDonnell, R.A. (1998): Principles of Geographical Information Systems. 2nd Edition, Oxford University Press.

CORINE (1992): *Soil Erosion Risk and Important Land Resources in the Southern Regions of the European Community*. EUR 13233, Luxembourg.

Daroussin, J. & King, D. (1996): A pedotransfer rules database to interpret the Soil Geographical Database of Europe for environmental purposes. *Proceedings of the workshop on the use of pedotransfer in soil hydrology research in Europe, Orléans, France, 10-123 October 1996.*

De Jong, S.M. (1994). Applications of reflective remote sensing for land degradation studies in a mediterranean environment. Nederlandse geografische studies 177.

De Jong, S.M., Brouwer, L.C. & Riezebos, H. Th. (1998): Erosion hazard assessment in the Peyne catchment, France. Working paper DeMon-2 Project. Dept. Physical Geography, Utrecht University.

De Ploey, J. (1989): *A Soil Erosion Map for Western Europe.* Catena Verlag.

De Roo, A.P.J. (1993): *Modelling Surface Runoff and Soil Erosion in Catchments Using Geographical Information Systems; Validity and Applicability of the 'ANSWERS' Model in Two Catchments in the Loess Area of South Limburg (The Netherlands) and one in Devon (UK).* Nederlandse Geografische Studies 157.

Desmet, P.J.J. & Govers, G. (1996). A GIS procedure for automatically calculating the USLE LS factor on topographically complex landcape units. *Journal of soil and water conservation 51*, p. 427-433.

Fournier, (1972). Soil Conservation - *Nature and Environment No 5*, Council of Europe, Strasbourg.

Heineke, H.J., Eckelmann, W., Thomasson, A.J., Jones, R.J.A., Montanarella, L. and Buckley, B. (eds) (1998). *Land Information Systems: Developments for planning the sustainable use of land resources*. EUR 17729 EN, 546pp. Office for Official Publications of the European Communities, Luxembourg

Jäger, S. (1994): Modelling Regional Soil Erosion Susceptibility Using the Universal Soil Loss Equation and GIS. In: Rickson, R.J (ed). *Conserving Soil Resources. European Perspectives*, pp. 161-177. CAB International.

King, D., Stengel, P. & Jamagne, M. (1999). Soil Mapping and Soil Monitoring: State of Progress and Use in France. In: Bullock, P., Jones, R.J.A. & Montanarella, L. (eds): *Soil Resources of Europe.* EUR 18991 EN, 204 pp. Office for Official Publications of the European Communities, Luxembourg.

Kirkby, M.J. & King, D (1998). *Summary report on provisional RDI erosion risk map for France*. Report on contract to the European Soil Bureau (unpublished)

Mitasova, H., Hofierka, J., Zlocha, M., Iverson, L.R. (1996). Modeling topographic potential for erosion and deposition using GIS. *International Journal of GIS 10*, p.629-642.

Montier, C., Daroussin, J., King, D. & Le Bissonnais, Y. (1998): *Cartographie vde l'aléa "Erosion des Sols" en France*. INRA, Orléans.

Moore, I.D. & Burch, G.J. (1986). Modeling erosion and deposition: Topographic effects. *Transactions ASAE 29*, p. 1624-1640.

Moore, I.D., Turner, A.K., Wilson, J.P., Jenson, S.K. & Band, L.E. (1993). GIS and land-surface-subsurface process modeling. In: Goodchild, M.FR., Parks, B.O. & Steyaert, L.T. (eds): *Environmental modeling with GIS*, p. 196-230.

Morgan, R.P.C. (1992). *Soil Erosion in the Northern Countries of the European Community*. EIW Workshop: Elaboration of a Framework of a Code of Good Agricultural Practices, Brussels, 21-22 May 1992.

Morgan, R.P.C. (1995): *Soil Erosion and Conservation. Second Edition.* Longman, Essex.

Morgan, R.P.C, Morgan, D.D.V. & Finney, H.J. (1984). A predictive model for the assessment of soil erosion risk. *Journal of agricultural engineering research 30,* p. 245-253.

Oldeman, L.R., Hakkeling, R.T.A. and Sombroek, W.G. (1991). *World Map of the Status of Human-Induced Soil Degradation, with Explanatory Note* (second revised edition) - ISRIC, Wageningen; UNEP, Nairobi.

Renard, K.G., Foster, G.R., Weessies, G.A., McCool, D.K., Yoder, D.C. (eds) (1997). *Predicting Soil Erosion by Water: A guide to to conservation planning with the Revised Universal Soil Loss Equation (RUSLE).* U.S. Department of Agriculture, Agriculture Handbook 703.

Rijks, D., Terres, J.M. & Vossen, P. (eds) (1998). *Agrometeorological applications for regional crop monitoring and production assessment*. EUR 17735 EN, 505 pp. Office for Official Publications of the European Communities, Luxembourg

Römkens (1985). The soil erodibility factor: a perspective. In: El-Swaify, S.A., W.C. Moldenhauer, A. Lo (eds.) (1985). S*oil erosion and conservation*.

Römkens, M.J.M, Prasad, S.N. & Poesen, J.W.A. (1986). Soil erodibility and properties. *Trans. 13th congress of the Int. Soc. Of Soil Sci., Hamburg, Germany* 5, p. 492-504.

Torri, D., Poesen, J. & Borselli, L. (1997). Predictability and uncertainty of the soil erodibility factor using a global dataset. *Catena* 31, p. 1-22.

Van Lynden, G.W.J. (1995). European soil resources*. Nature and Environment No. 71*. Council of Europe, Strasbourg.

Wischmeier, W.H. & Smith, D.D. (1978). *Predicting rainfall erosion losses –a guide for conservation planning*. U.S. Department of Agriculture, Agriculture Handbook 537

Yassoglou, N., Montanarella, L., Govers, G., Van Lynden, G., Jones, R.J.A., Zdruli, P., Kirkby, M., Giordano, A., Le Bissonnais, Y., Daroussin, J. & King, D. (1998): *Soil Erosion in Europe.* European Soil Bureau.